

SO(5) critical point in a spin-flavor Kondo device: Bosonization and refermionization solution

 Alon Liberman¹, Andrew K. Mitchell,^{2,3} Ian Affleck,⁴ and Eran Sela¹
¹*School of Physics and Astronomy, Tel Aviv University, Tel Aviv 6997801, Israel*
²*School of Physics, University College Dublin, Belfield, Dublin 4, Ireland*
³*Centre for Quantum Engineering, Science, and Technology, University College Dublin, Belfield, Dublin 4, Ireland*
⁴*Department of Physics and Astronomy and Stewart Blusson Quantum Matter Institute, University of British Columbia, Vancouver, British Columbia, Canada V6T 1Z1*


(Received 17 March 2021; revised 29 April 2021; accepted 29 April 2021; published 14 May 2021)

We investigate a well-studied system of a quantum dot coupled to a Coulomb box and leads, realizing a spin-flavor Kondo model. It exhibits a recently discovered non-Fermi liquid (NFL) behavior with emergent SO(5) symmetry. Here, through a detailed bosonization and refermionization solution, we push forward our previous work and provide a consistent and complete description of the various exotic properties and phase diagram. A unique NFL phase emerges from the presence of an uncoupled Majorana fermion from the flavor sector, whereas Fermi liquid-like susceptibilities result from the gapping out of a pair of Majorana fermions from the spin and flavor sectors. Other properties, such as a $T^{3/2}$ scaling of the conductance, stability under channel or spin-symmetry breaking, and a reappearance of NFL behavior upon breaking the particle-hole symmetry, are all accounted for by a renormalization group treatment of the refermionized Majorana model.

 DOI: [10.1103/PhysRevB.103.195131](https://doi.org/10.1103/PhysRevB.103.195131)
I. INTRODUCTION

Quantum dots (QDs) are among the most basic building blocks of mesoscopic circuits [1], providing a testbed for strongly correlated and entangled problems within the simple context of a quantum impurity model. The physical properties of QDs depend essentially on their level spacing δ , charging energy E_c , and precise form of the coupling to their surroundings: They can exhibit Coulomb blockade phenomena at low temperatures [2] $T \ll E_c$ and build up entangled Kondo-like states of various kinds [3–6] below the Kondo temperature $T \ll T_K$. Within the Coulomb blockade regime, one may either have small QDs dominated by a single quantum level due to a large level spacing $\delta \gg T$, or large QDs which are metallic grains with $\delta \ll T$, referred to here as “Coulomb boxes,” having a large density of states, yet displaying charge quantization [7,8].

This combination of large charging energy and large density of states has been a central ingredient in the first experimental realization of the two-channel Kondo (2CK) effect [9–11]. Here, multiple Coulomb boxes act as effective screening channels of a small central QD carrying an unpaired spin, and the boxes’ charging energy completely suppresses interchannel charge transfer. Its exotic non-Fermi liquid (NFL) behavior is reflected in nontrivial electronic scattering properties which were calculated using conformal field theory (CFT) [12] accounting for anomalous experimental signatures [10,11].

These experiments opened a line of research activity on the quantum critical nature of this NFL state [13–17], the role of charge fluctuations near charge degeneracy of the Coulomb box [18–20], the nonlocal role of the Coulomb charging energy [21], various transport [22–25] and capacitance [26] properties, and multiple impurities generalizations [27] and

related devices [28]. Also, the nontrivial entropy of these models was recognized as a possible way to realize non-Abelian anyons [29,30]. More recently, Coulomb boxes were implemented in the strong-magnetic-field regime [31–33] leading to a convenient experimental platform to study multichannel charge-Kondo effects achieved near charge degeneracy points of the Coulomb box [8,32,34–38].

The lead-dot-box device of Refs. [9–11] on which we focus (see Fig. 1) exhibits a rich phase diagram invoking correlations between spin and charge degrees of freedom, as a function of gate parameters controlling the charges of the box and small QD. In particular, a certain tuning of parameters gives rise to a spin-flavor Kondo effect: a phase in which the spin-1/2 formed in the small QD, \vec{S} , gets entangled with a “flavor” pseudospin-1/2 operator \vec{T} , associated with two charge states of the box.

To model the lead-dot-box system in Fig. 1 we study the low-energy Hamiltonian $H_0 + \delta H$, where $H_0 = \sum_k \sum_{\alpha=L,B,\sigma=\uparrow,\downarrow} \epsilon_k c_{k\alpha\sigma}^\dagger c_{k\alpha\sigma}$ describes the leads ($\alpha = L$) or the box ($\alpha = B$), respectively, and

$$\begin{aligned} \delta H = & \sum_{a=x,y,z} J \psi^\dagger \frac{\sigma^a}{2} \psi S^a + \sum_{b=x,y,z} V_b \psi^\dagger \frac{\tau^b}{2} \psi T^b \\ & + \sum_{a,b=x,y,z} Q_b \psi^\dagger \sigma^a \tau^b \psi S^a T^b, \\ Q_x = Q_y \equiv Q_\perp, \quad V_x = V_y \equiv V_\perp. \end{aligned} \quad (1)$$

Here Pauli matrices σ^a and τ^b act in the spin and flavor sectors, respectively. In Eq. (1) we suppress spin and flavor indices; for example, $\psi^\dagger \sigma^a \tau^b \psi \equiv \sum_{\alpha,\beta,\sigma,\sigma'} \psi_{\alpha\sigma}^\dagger \sigma_{\sigma\sigma'}^a \tau_{\alpha\beta}^b \psi_{\beta\sigma'}$, where we define local field operators $\psi_{\alpha\sigma} = \sum_k c_{k\alpha\sigma}$. In this paper, we study the rich phase diagram of this Hamiltonian with a number of additional perturbations.

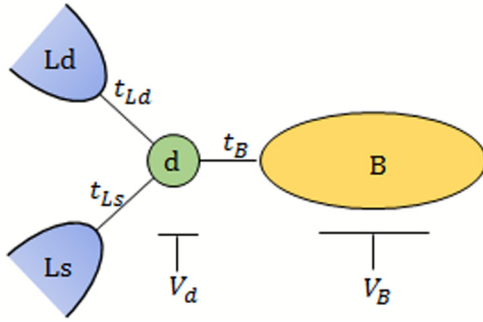


FIG. 1. A quantum dot (d) coupled to a quantum box (B) and source and drain leads (Ls and Ld).

Previous results and emergent symmetry

An earlier work on this model by Borda *et al.* [39] found that at low energies, the ratios between the various coupling constants J , Q_b , and V_b ($b = x, y, z = 1, 2, 3$) flow under renormalization group (RG) to unity. Remarkably, the resulting low-temperature fixed point has an enlarged SU(4) symmetry. Using numerical RG (NRG) and CFT it was found that this SU(4) symmetric state is a stable Fermi liquid (FL). This high-symmetry state is featured in a number of QD experiments [40–42] and theories [43–45].

Le Hur *et al.* [18,19] explored the consequences of this stable SU(4) FL state on the conductance and capacitance. The model in Fig. 1 was also elaborated on in a series of papers by Anders, Lebanon, and Schiller (ALS) [46–48]. They focused on the particle-hole (PH) symmetric case and found a NFL ground state, rather than a FL behavior claimed by Le Hur *et al.* Also, ALS found a smooth crossover from spin to flavor 2CK NFL behavior as a function of the box’s gate voltage.

Below, these two seemingly conflicting results will be reconciled by the introduction of a NFL fixed point, located at the PH symmetric point and characterized by an SO(5) symmetry [49], exhibiting both FL-like susceptibilities and NFL fractional entropy, along with a $T^{\frac{3}{2}}$ scaling of the conductance. While the key features of this SO(5) fixed point were found in Ref. [49], here we provide a detailed analysis of the phase diagram and interplay of different perturbations.

Our main endeavor is the investigation of this unique SO(5) point along with its stability to the following perturbations: magnetic field ($\Delta H_B = BS^z$), flavor field ($\Delta H_{B_f} = B_f T^z$), channel symmetry breaking ($\Delta H_{as} = J_- \psi^\dagger \frac{\sigma_x \tau^z}{2} \psi \vec{S}$), and PH symmetry breaking [nonzero V_\perp and Q_z in Eq. (1)]. We show that the NFL phase at the SO(5) point is stable to the inclusion of a magnetic field or channel symmetry breaking. While this stability of the NFL state is reflected by a fractional entropy of $\frac{1}{2} \log 2$, other quantities such as the spin susceptibility show FL-like behavior [18,19] of an inherently NFL state.

The addition of PH symmetry breaking including a flavor field, however, can destabilize the NFL to a FL. Interestingly, when both destabilizing perturbations occur, it is still possible to tune them to cancel each other and restabilize a NFL phase, which persists along a curve in the plane spanned by the PH symmetry breaking perturbation and flavor field perturbation (bold curve in Fig. 2). In the QD device in Fig. 1

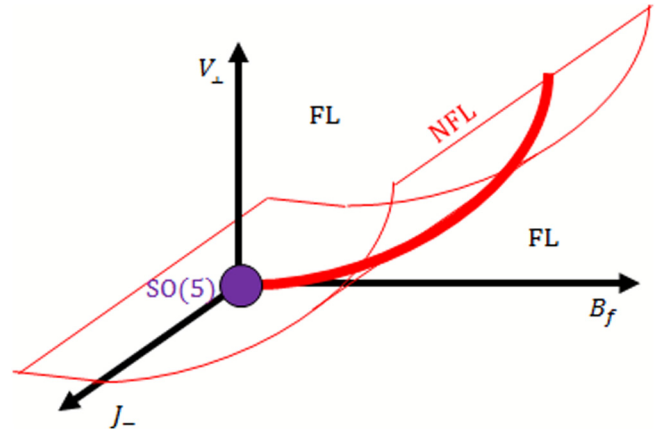


FIG. 2. A schematic drawing of the NFL line (in bold) emanating from the SO(5) fixed point in the plane spanned by B_f and V_\perp perturbations. The NFL line becomes a NFL 2D manifold as we add the J_- term as a third perturbation. We describe this curve explicitly in Sec. VI using Eq. (61).

this corresponds to a curve in the phase diagram spanned by the gate voltages V_d and V_B (drawn in Fig. 5 for different parameter choices). Adding a third axis representing, e.g., ΔH_{as} , results in a two-dimensional (2D) NFL manifold in Fig. 2. This means that the NFL line in the phase diagram exists for generic ratios between the tunneling coefficients of the leads and the box [49].

We also note that related works on the spin-flavor Kondo model [50–52], which used bosonization and refermionization methods as in the present paper, did not focus on the special role of PH symmetry to be elucidated below, which stabilizes the high-symmetry SO(5) NFL fixed point.

The plan of the paper is as follows. In Sec. II we present the lead-dot-box Hamiltonian and map it to the low-energy form of Eq. (1) by the Schrieffer-Wolff transformation. We examine the system’s RG behavior with and without PH-symmetry-breaking terms, and make the emergent symmetry explicit. In Sec. III we apply bosonization and refermionization techniques, obtaining a Majorana representation of the problem. In Sec. IV, we analyze the spin-flavor phase at the SO(5) point in terms of thermodynamic quantities (entropy, spin, and flavor susceptibilities) and conductance. In Sec. V, we explore how these quantities change under different perturbations, and in Sec. VI we combine PH-symmetry-breaking perturbations to show the emergence of a NFL line from the SO(5) point in the phase diagram. Our field theory results in Secs. V and VI are compared with our NRG calculations. We briefly conclude in Sec. VII.

II. MODEL

A. Lead-dot-box model

As shown in Fig. 1, our system, studied in numerous earlier works [9,13,19,20], consists of a central QD (d) connected to source and drain leads (Ls , Ld), and to a quantum box (B). It is described by the Hamiltonian $H = H_0 + H_B + H_d + H_{\text{hyb}}$. The hybridization term $H_{\text{hyb}} = \sum_\alpha H_{\text{hyb}}^\alpha$ couples the small dot with the various reservoirs. Here $H_0 = \sum_{k,\alpha,\sigma} \epsilon_k c_{k\alpha\sigma}^\dagger c_{k\alpha\sigma}$

TABLE I. Summary of interaction terms, their couplings, their LR and PH symmetries, their RG role with respect to the SO(5) fixed point, and their Majorana fermion form.

Interaction, \mathcal{O}_j	Coupling	LR symmetry	PH symmetry	Role	EK form
$\psi^\dagger \frac{\bar{\sigma}}{2} \psi \bar{S}$	J	+	+	SO(5)	$\approx id_- \chi_+$
$T^z \psi^\dagger \frac{\tau^z}{2} \psi$	V_z	+	+	SO(5)	
$\psi^\dagger \frac{\bar{\sigma}}{2} (\tau^- T^+ - \tau^+ T^-) \psi \bar{S}$	Q_\perp	+	+	SO(5)	$\approx id_+ a_-$
$\psi^\dagger \frac{\tau^+ T^- - \tau^- T^+}{2} \psi$	V_\perp	+	-	\rightarrow SU(4)	$\approx ia_+ \chi_-$
$T^z \psi^\dagger \bar{\sigma} \tau^z \psi \bar{S}$	Q_z	+	-	\rightarrow SU(4)	$\approx ia_+ \chi_-$
$\psi^\dagger \psi$	ϕ	+	-	marginally irrelevant	
$\psi^\dagger \frac{\bar{\sigma} \tau^z}{2} \psi \bar{S}$	J_-	-	+	marginal	$\approx id_+ \chi_-$
$T^z \psi^\dagger \bar{\sigma} \psi \bar{S}$	Q_z^-	-	-	irrelevant	
$\frac{1}{2} T^z \psi^\dagger \psi$	V_z^-	-	+	irrelevant	
$\psi^\dagger \tau^z \psi$	ϕ_-	-	-	marginal	$\approx ia_- a_+$
T^z	B_f	-	-	marginal	$\approx ia_- a_+$

describes the three conduction electron reservoirs, consisting of the two leads ($\alpha = Ls, Ld$) plus the one box ($\alpha = B$) that surround the small quantum dot. In addition,

$$H_B = E_c (\hat{N}_B - N_0 - n_g)^2, \quad (2)$$

$$H_d = \epsilon_d n_d + U n_\uparrow n_\downarrow, \quad (3)$$

describe the box Coulomb interaction and the Hamiltonian of the small dot, respectively, and the hybridization term is given by $H_{\text{hyb}}^\alpha = \sum_{k,\sigma} (t_{k\alpha} d_\sigma^\dagger c_{k\alpha\sigma} + \text{H.c.})$. Here, $\sigma = \uparrow, \downarrow$ denotes (real) spin, and d_σ or $c_{k\alpha\sigma}$ are annihilation operators for the dot or conduction electrons, respectively. $n_\sigma = d_\sigma^\dagger d_\sigma$ and $n_d = \sum_\sigma n_\sigma$ measure the number of electrons in the dot, and $\hat{N}_B = \sum_{k,\sigma} c_{kB\sigma}^\dagger c_{kB\sigma}$ is the number operator for the box.

The dot and box occupations are controllable by gate voltages

$$V_d \propto \eta = \epsilon_d + \frac{1}{2}U, \quad V_B \propto n_g - \frac{1}{2}, \quad (4)$$

respectively (see Fig. 1). We take equivalent conduction electron baths $\epsilon_{\alpha k} \equiv \epsilon_k$ with a constant density of states ν (which we set to unity). We define $t_\alpha^2 = \sum_k |t_{\alpha k}|^2$ and $t_L^2 = t_{Ls}^2 + t_{Ld}^2$. The two leads can be effectively treated as a single lead. Thus, the combined lead (L) and box (B) act as two channels [13]. We will often refer to the lead and box as the left (L) and right (R) channels. At $n_g = \frac{1}{2}$, the box states with N_0 and $N_0 + 1$ electrons are degenerate. Neglecting other high-energy box charge states we may define a pseudospin- $\frac{1}{2}$ operator $T^+ = |N_0 + 1\rangle \langle N_0|$, $T^- = (T^+)^{\dagger}$, and $T^z = \frac{1}{2}(|N_0 + 1\rangle \langle N_0 + 1| - |N_0\rangle \langle N_0|)$. The charge pseudospin is flipped by electronic tunneling between the dot and box. The lead-dot-box Hamiltonian is then

$$H_{\text{ALS}} = \sum_{\alpha=L,R} \sum_{k,\sigma} \epsilon_k c_{k\alpha\sigma}^\dagger c_{k\alpha\sigma} + E_c (T^z + 1/2 - n_g)^2 + H_d + \sum_{k,\sigma} [d_\sigma^\dagger (t_L c_{kL\sigma} + t_B c_{kB\sigma} T^-) + \text{H.c.}]. \quad (5)$$

We refer to this model in which the tunneling terms are supplemented by the T -pseudospin operator as the ALS model.

B. PH transformation

In the next section we map the lead-dot-box model to the spin-flavor Kondo model, Eq. (1), perturbed by various terms. Before doing so, we introduce a PH transformation allowing us to distinguish various interactions. The PH transformation takes

$$\begin{aligned} \psi &\rightarrow \sigma^y \psi^\dagger, & d &\rightarrow -\sigma^y d^\dagger, \\ T^+ &\rightarrow T^-, & T^z &\rightarrow -T^z. \end{aligned} \quad (6)$$

For example, this symmetry takes $\psi^\dagger \tau^z \psi \rightarrow -\psi^\dagger \tau^z \psi$ so the $(\psi^\dagger \tau^z \psi) T^z$ term (associated with the V_z coupling) respects the symmetry since T^z also changes sign. On the other hand, it takes $\psi^\dagger \tau^+ \psi \rightarrow -\psi^\dagger \tau^- \psi$ and $T^+ \rightarrow T^-$ so the \pm -flavor Kondo terms (with coupling V_\perp) change sign and are PH odd. Importantly, this PH symmetry holds only when both conditions $\epsilon_d = -U/2$ and $n_g = 1/2$ hold. It is easy to check that also Q_z in Eq. (1) is odd under PH symmetry. Table I summarizes the PH transformation of the various operators in Eq. (1) as well as other perturbations that we discuss next.

C. Schrieffer-Wolff (SW) transformation

We expand the Hamiltonian at low temperatures $T \ll E_c, U$ around the two possible box charge states $N_0, N_0 + 1$, and around the two spin states of the small dot, using the SW transformation [53]. To second order one generates the terms that appear in Table I, which consist of the Hamiltonian

$$H = H_0 + \delta H(J, V_z, V_\perp, Q_z, Q_\perp) + \delta H_{ps}(\phi) + \Delta H_{B_f}(B_f) + \Delta H_B(B) + \delta H_-(J_-, V_z^-, Q_z^-, \phi_-). \quad (7)$$

Here, δH was introduced in Eq. (1). $\Delta H_{B_f} = B_f T^z$ describes a flavor field, namely, an energy difference between the charge states of the box,

$$B_f = E_c [(1 - n_g)^2 - n_g^2] = E_c (1 - 2n_g), \quad (8)$$

(to zero order in the tunneling). We also included a magnetic field term $\Delta H_B = B S^z$, which requires spin-symmetry breaking. $\delta H_{ps}(\phi) = \phi \psi^\dagger \psi$ is a potential scattering term.

All terms in δH_- break channel symmetry. We refer to the channel symmetry of exchanging the lead and box as a left-right (LR) symmetry (see Table I). This symmetry also takes $T^z \rightarrow -T^z$, and is satisfied in Eq. (1). Among the terms that break this symmetry in δH_- , specifically J_- describes an asymmetry in the spin-Kondo interaction.

We relegate full explicit expressions of the coupling constants to Appendix A. PH-even couplings such as J , Q_\perp , and V_z are generically finite, and specifically at the PH symmetric point $\epsilon_d = -U/2$, $n_g = 1/2$, are given by

$$J = \frac{4}{U} \left(t_L^2 + \frac{t_B^2(E_c + U/2)}{2E_c + U/2} \right), \quad Q_\perp = 4 \frac{t_L t_B}{U},$$

$$V_z = 4 \frac{E_c t_B^2}{U(2E_c + U/2)}.$$

On the other hand, the PH-odd couplings vanish at the PH symmetric point; for example, V_\perp takes the form

$$V_\perp = -t_L t_B \frac{E_c(2n_g - 1) + 2\epsilon_d + U}{(\epsilon_d + E_c(2n_g - 1))(\epsilon_d + U)}. \quad (9)$$

D. RG equations and emergent symmetries

In this section we consider the Hamiltonian $H + \delta H(J, V, Q)$. The analysis of the remaining terms, such as channel asymmetry, and magnetic and flavor fields, is postponed to Sec. V.

We have seen that, away from the PH symmetric point $(n_g, \eta) = (\frac{1}{2}, 0)$, generically all coupling constants J , V_z , V_\perp , Q_z , and Q_\perp in Eq. (1) are finite. They satisfy the following weak-coupling RG equations [19]:

$$\begin{aligned} \frac{dJ}{dl} &= J^2 + Q_z^2 + 2Q_\perp^2, \\ \frac{dV_z}{dl} &= V_\perp^2 + 3Q_\perp^2, \\ \frac{dV_\perp}{dl} &= V_\perp V_z + 3Q_\perp Q_z, \\ \frac{dQ_z}{dl} &= 2JQ_z + 2V_\perp Q_\perp, \\ \frac{dQ_\perp}{dl} &= 2JQ_\perp + V_z Q_\perp + V_\perp Q_z. \end{aligned} \quad (10)$$

Here l is the logarithmic RG scale parameter. In a similar fashion to the Kondo RG equations displaying the irrelevancy of spin anisotropy, it was noticed [19,39] that the present system of RG equations flows to a strong-coupling fixed point with equal couplings. When the system reaches isotropy $V = Q = J$, these RG equations become $dJ/dl = 4J^2$. The system flows to the upper fixed point in Fig. 3 on the Kondo scale [19]:

$$T_K^{\text{SU}(4)} \sim D e^{-1/4J}, \quad (11)$$

where D is the conduction electron's bandwidth.

Now consider the $(n_g, \eta) = (\frac{1}{2}, 0)$ point where $V_\perp = Q_z = 0$. A similar analysis of the isotropy of the remaining couplings J , V_z , and Q_\perp , suggests a flow to an isotropic fixed point (see lower fixed point in Fig. 3) with $dJ/dl = 3J^2$, and the partially isotropic Hamiltonian flows to the lower fixed point

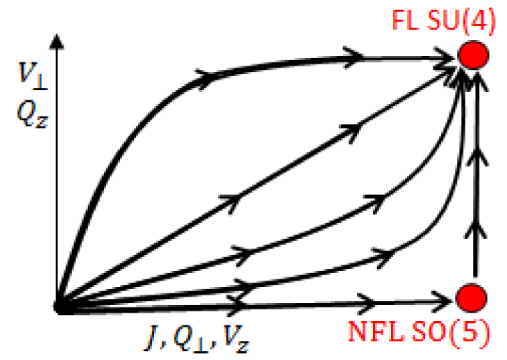


FIG. 3. Schematic RG flow for the PH-even couplings (horizontal axis) and PH-odd couplings (vertical axis). In the infrared, the couplings flow to one of two fixed points: a NFL phase or a FL phase. A quantum phase transition from the former to the latter distinct phases occurs as the PH-odd couplings are turned on.

in Fig. 3, with a slightly smaller Kondo scale,

$$T_K^{\text{SO}(5)} \sim D e^{-1/3J}. \quad (12)$$

I. SU(4) versus SO(5)

Consider the matrix of 15 generators:

$$T^{ab} = \frac{1}{2} \begin{pmatrix} 0 & \sigma^3 & -\sigma^2 & \sigma^1 \tau^1 & \sigma^1 \tau^2 & \sigma^1 \tau^3 \\ -\sigma^3 & 0 & \sigma^1 & \sigma^2 \tau^1 & \sigma^2 \tau^2 & \sigma^2 \tau^3 \\ \sigma^2 & -\sigma^1 & 0 & \sigma^3 \tau^1 & \sigma^3 \tau^2 & \sigma^3 \tau^3 \\ -\sigma^1 \tau^1 & -\sigma^2 \tau^1 & -\sigma^3 \tau^1 & 0 & \tau^3 & -\tau^2 \\ -\sigma^1 \tau^2 & -\sigma^2 \tau^2 & -\sigma^3 \tau^2 & -\tau^3 & 0 & \tau^1 \\ -\sigma^1 \tau^3 & -\sigma^2 \tau^3 & -\sigma^3 \tau^3 & \tau^2 & -\tau^1 & 0 \end{pmatrix}. \quad (13)$$

The 15 independent generators appearing in the upper triangular part ($T^{ab} = -T^{ba}$ with $a, b = 1, \dots, 6$) satisfy the algebra $[T^{ab}, T^{cd}] = -i(\delta_{bc} T^{ad} - \delta_{ac} T^{bd} - \delta_{bd} T^{ac} + \delta_{ad} T^{bc})$. Hence [54] they are 15 generators of $\text{SO}(6)$, which is isomorphic to $\text{SU}(4)$. Specifically, these matrices form a four-dimensional representation.

We can organize the impurity operators S and T into generators of this $\text{SO}(6)$ symmetry. One introduces a singly occupied fermionic site carrying spin and flavor indices [55], $f_{\alpha\sigma}^\dagger f_{\alpha\sigma} = 1$, in terms of which $S^a = f_{\alpha\sigma}^\dagger \frac{\sigma^a}{2} f$, $T^b = f_{\alpha\sigma}^\dagger \frac{\tau^b}{2} f$, and $2S^a T^b = f_{\alpha\sigma}^\dagger \frac{\sigma^a \tau^b}{2} f$. Then the four impurity states form a representation of $\text{SO}(6)$:

$$\begin{aligned} f^\dagger T^{ab} f &= M^{ab} \\ &= \begin{pmatrix} 0 & S^z & -S^y & 2S^x T^x & 2S^x T^y & 2S^x T^z \\ -S^z & 0 & S^x & 2S^y T^x & 2S^y T^y & 2S^y T^z \\ S^y & -S^x & 0 & 2S^z T^x & 2S^z T^y & 2S^z T^z \\ -2S^x T^x & -2S^y T^x & -2S^z T^x & 0 & T^z & -T^y \\ -2S^x T^y & -2S^y T^y & -2S^z T^y & -T^z & 0 & T^x \\ -2S^x T^z & -2S^y T^z & -2S^z T^z & T^z & -T^x & 0 \end{pmatrix}. \end{aligned} \quad (14)$$

Evidently, the fully isotropic situation with $J = V_z = V_\perp = Q_z = Q_\perp$ allows us to write Hamiltonian $H + \delta H$ in Eq. (1)

in SO(6) [or equivalently SU(4)] isotropic form,

$$H_{\text{SO}(6)} = H_0 + J \sum_{A=1}^{15} J^A M^A, \quad (15)$$

where $J^A = \psi^\dagger T^A \psi$ and $\sum_{A=1}^{15} = \sum_{a<b, a, b=1}^6$.

The case with PH symmetry in our model corresponds to $V_\perp = Q_z = 0$. Then the Hamiltonian (1) can be written in terms of the ten generators of SO(5), which is a subgroup of SO(6). These ten generators are given by T^{ab} with $a, b = 1, \dots, 5$ [given by the matrix in Eqs. (14) by removing the last column and row],

$$H_{\text{SO}(5)} = H_0 + J \sum_{A=1}^{10} J^A M^A, \quad (16)$$

where $\sum_{A=1}^{10} = \sum_{a<b, a, b=1}^5$.

2. Generalized anisotropic RG equations

The RG equations (10) assumed spin SU(2) symmetry as reflected, e.g., in the Kondo coupling J . Similarly it assumed flavor U(1) symmetry implying $V_x = V_y$ and $Q_x = Q_y$. Motivated by the next section based on the anisotropic Emery-Kivelson approach, in which the spin SU(2) symmetry is broken, we now generalize the RG equations to the fully anisotropic case of the form $H_0 + \sum_{a<b, a, b=1}^6 \lambda_{ab} (\psi^\dagger T^{ab} \psi) (f^\dagger T^{ab} f)$. We associate each of these terms with a coupling λ_{ab} :

$$\lambda_{ab} = \begin{pmatrix} 0 & J_z & J_y & Q_x^x & Q_y^x & Q_z^x \\ J_z & 0 & J_x & Q_x^y & Q_y^y & Q_z^y \\ J_y & J_x & 0 & Q_x^z & Q_y^z & Q_z^z \\ Q_x^x & Q_y^y & Q_z^z & 0 & V_z & V_y \\ Q_x^y & Q_y^x & Q_z^z & V_z & 0 & V_x \\ Q_x^z & Q_y^z & Q_z^z & V_y & V_x & 0 \end{pmatrix}. \quad (17)$$

Here, we defined Q_b^a by generalizing the spin-flavor coupling terms Q_b in Eq. (1) to $Q_b^a \psi^\dagger \sigma^a \tau^b \psi S^a T^b$, yielding 15 independent coupling constants. As demonstrated in Appendix C, these 15 coupling constants satisfy the RG equation

$$\frac{d\lambda_{ij}}{dl} = \sum_{k \neq i, j} \lambda_{ik} \lambda_{kj}. \quad (18)$$

For example, the RG flow of J_x is given by

$$\begin{aligned} \frac{dJ_x}{dl} &= \frac{d\lambda_{23}}{dl} = \lambda_{21}\lambda_{13} + \lambda_{24}\lambda_{43} + \lambda_{25}\lambda_{53} + \lambda_{26}\lambda_{63} \\ &= J_z J_y + Q_x^y Q_x^z + Q_y^y Q_y^z + Q_z^y Q_z^z. \end{aligned} \quad (19)$$

This system of equations is numerically solved in Appendix C, showing that the isotropic fixed point is achieved for anisotropic bare values including spin anisotropy, which corresponds to the Toulouse limit discussed in the next section.

III. MAPPING TO A MODEL OF MAJORANA FERMIONS

A. Bosonization and refermionization

In this section we apply the techniques that Emery and Kivelson (EK) employed to the spin-2CK model [56], to solve

our spin-flavor model [Eq. (1)]. The resulting model consists of a fixed-point Hamiltonian which is quadratic in terms of bulk and local Majorana fermions. While in this section we present the mapping to the various terms of the Hamiltonian into the Majorana description, in Sec. IV we will apply this approach to construct the phase diagram.

As discussed in detail in Refs. [57,58], the starting point is to write the free part of the Hamiltonian in terms of chiral one-dimensional fermions, $H_0 = \sum_{\alpha, \sigma} i v_F \int_{-\infty}^{\infty} \frac{dx}{2\pi} \psi_{\alpha\sigma}^\dagger \partial_x \psi_{\alpha\sigma}$, where v_F is the Fermi velocity. We now treat the various perturbations. We first consider the terms $H_J + H_{V_z}$, i.e., (i) the spin-Kondo interactions in Eq. (1) which we assume to be anisotropic,

$$\begin{aligned} H_J &= \frac{1}{2} J_z S^z (\psi_{\alpha\uparrow}^\dagger \psi_{\alpha\uparrow} - \psi_{\alpha\downarrow}^\dagger \psi_{\alpha\downarrow}) \\ &+ \frac{1}{2} J_\perp (S^+ \psi_{\alpha\downarrow}^\dagger \psi_{\alpha\uparrow} + S^- \psi_{\alpha\uparrow}^\dagger \psi_{\alpha\downarrow}), \end{aligned} \quad (20)$$

together with (ii) the V_z term $H_{V_z} = \frac{1}{2} V_z T^z \psi^\dagger \tau^z \psi$.

The EK transformation begins with the replacement of the fermionic fields $\psi_{\alpha\sigma}(x)$ with bosonic fields $\phi_{\alpha\sigma}(x)$, using the relation

$$\psi_{\alpha\sigma}(x) = F_{\alpha\sigma} a^{-1/2} e^{-i\phi_{\alpha\sigma}(x)}. \quad (21)$$

Here a is a short distance cutoff [57,59] which we set to unity. The Klein factors $F_{\alpha\sigma}$ retain the fermionic commutation relations. The spin-flip Kondo term becomes

$$H_{J_\perp} = \frac{1}{2} J_\perp (S^+ F_{\alpha\downarrow}^\dagger F_{\alpha\uparrow} e^{i\phi_{\alpha\downarrow}} e^{-i\phi_{\alpha\uparrow}} + \text{H.c.}). \quad (22)$$

We then use the bosonization identity [58] $\psi_{\alpha\sigma}^\dagger(x) \psi_{\alpha\sigma}(x) = \partial_x \phi_{\alpha\sigma}(x)$ to bosonize the J_z term,

$$H_{J_z} = \frac{1}{2} J_z S^z (\partial_x \phi_{\alpha\uparrow} - \partial_x \phi_{\alpha\downarrow}). \quad (23)$$

Likewise, the free Hamiltonian maps to $H_0 = \sum_{\alpha\sigma} v_F \int_{-\infty}^{\infty} \frac{dx}{2\pi} \frac{1}{2} (\partial_x \phi_{\alpha\sigma})^2$. Next, the bosonic fields $\phi_{\alpha\sigma}$ are reexpressed in a basis of charge, spin, flavor, and spin-flavor degrees of freedom, denoted by $\phi_{\mathcal{A}}$ ($\mathcal{A} = c, s, f, sf$):

$$\begin{aligned} \phi_c &= \frac{1}{2} (\phi_{1\uparrow} + \phi_{1\downarrow} + \phi_{2\uparrow} + \phi_{2\downarrow}), \\ \phi_s &= \frac{1}{2} (\phi_{1\uparrow} - \phi_{1\downarrow} + \phi_{2\uparrow} - \phi_{2\downarrow}), \\ \phi_f &= \frac{1}{2} (\phi_{1\uparrow} + \phi_{1\downarrow} - \phi_{2\uparrow} - \phi_{2\downarrow}), \\ \phi_{sf} &= \frac{1}{2} (\phi_{1\uparrow} - \phi_{1\downarrow} - \phi_{2\uparrow} + \phi_{2\downarrow}). \end{aligned} \quad (24)$$

Thus

$$\begin{aligned} H_0 + H_J &= v_F \int_{-\infty}^{\infty} \frac{dx}{2\pi} \frac{1}{2} (\partial_x \phi_s)^2 + J_z S^z \partial_x \phi_s(0) \\ &+ \frac{1}{2} J_\perp S^+ e^{-i\phi_s} [F_{1\downarrow}^\dagger F_{1\uparrow} e^{-i\phi_{sf}(0)} + F_{2\downarrow}^\dagger F_{2\uparrow} e^{i\phi_{sf}(0)}] + \text{H.c.} \end{aligned} \quad (25)$$

We proceed to perform unitary rotations generated by the S^z and T^z operators,

$$U = e^{i(\gamma_s S^z \phi_s + \gamma_f T^z \phi_f)}. \quad (26)$$

In the spin-flip term J_\perp , the spin ladder operators transform as $S_\pm \rightarrow S_\pm e^{\pm i\gamma_s \phi_s}$, yielding

$$\begin{aligned} H_0 + H_J + H_{V_z} &\rightarrow \\ H_0 + \frac{1}{2} J_\perp (S^+ e^{i\gamma_s \phi_s}) e^{-i\phi_s} [F_{1\downarrow}^\dagger F_{1\uparrow} e^{-i\phi_{sf}} \\ &+ F_{2\downarrow}^\dagger F_{2\uparrow} e^{+i\phi_{sf}}] + \text{H.c.} \\ &+ (J_z - \gamma_s v_F) S^z \partial_x \phi_s + (V_z - \gamma_f v_F) T^z \partial_x \phi_f. \end{aligned} \quad (27)$$

A particular choice of the anisotropy parameters J_z and V_z , satisfying

$$\gamma_s = \frac{J_z}{v_F}, \quad \gamma_f = \frac{V_z}{v_F} \quad (\text{Toulouse point}), \quad (28)$$

results in a cancellation of the last two lines in Eq. (27). In addition, the vertex parts $e^{-i\phi_A}$ of both spin and flavor sectors cancel in all Kondo interactions, including those of the Q and V operators, if $\gamma_s = \gamma_f = 1$.

The spin-flip term becomes

$$\frac{1}{2} J_\perp S^+ [F_{1\downarrow}^\dagger F_{1\uparrow} e^{-i\phi_{sf}} + F_{2\downarrow}^\dagger F_{2\uparrow} e^{+i\phi_{sf}}] + \text{H.c.} \quad (29)$$

We proceed to define new Klein operators expressed in the basis of $\mathcal{A} = c, s, f, sf$, satisfying the following relations [57,59]:

$$\begin{aligned} F_x^\dagger F_s^\dagger &\equiv F_{\uparrow 1}^\dagger F_{\downarrow 1}, \quad F_x F_s^\dagger \equiv F_{\uparrow 2}^\dagger F_{\downarrow 2}, \\ F_x^\dagger F_f^\dagger &\equiv F_{\uparrow 1}^\dagger F_{\uparrow 2}, \quad F_x F_f^\dagger \equiv F_{\uparrow 1}^\dagger F_{\uparrow 2}^\dagger. \end{aligned} \quad (30)$$

Then the spin-flip term becomes

$$H_{J_\perp} = \frac{1}{2} J_\perp S^+ [F_s (F_{sf} e^{-i\phi_{sf}} + F_{sf}^\dagger e^{i\phi_{sf}})] + \text{H.c.} \quad (31)$$

Finally we refermionize, i.e., rewrite these interactions in terms of the new fermionic operators (either local or bulk fermions),

$$\psi_{\mathcal{A}}(x) = F_{\mathcal{A}} e^{-i\phi_{\mathcal{A}}(x)} \quad (\mathcal{A} = c, s, f, sf), \quad (32)$$

$$d = F_s^\dagger S^-, \quad a = F_f^\dagger T^-, \quad (33)$$

where $\psi_{\mathcal{A}}$ are bulk fermions and d, a are local fermions, corresponding to the spin and flavor impurity degrees of freedom, respectively. The bulk fermions can be used to define Majorana fermion fields evaluated at $x = 0$,

$$\chi_{\mathcal{A}+} \equiv \frac{\psi_{\mathcal{A}}^\dagger + \psi_{\mathcal{A}}}{\sqrt{2}}, \quad \chi_{\mathcal{A}-} \equiv \frac{\psi_{\mathcal{A}}^\dagger - \psi_{\mathcal{A}}}{i\sqrt{2}}. \quad (34)$$

We also define local Majorana fermions (“Majoranas”)

$$a_+ \equiv \frac{a^\dagger + a}{\sqrt{2}}, \quad a_- \equiv \frac{a^\dagger - a}{i\sqrt{2}}, \quad (35)$$

and similarly for d_\pm . Notice that $a^\dagger a = \frac{1}{2} + T^z = \frac{1}{2} + ia_- a_+$ and $a_\pm^2 = \frac{1}{2}$ (and similarly for d_\pm).

Thus, after the EK transformation we ended up with (i) four local Majoranas, accounting for the $2 \log 2$ impurity entropy of the free fermion fixed point, due to the spin and flavor impurity degrees of freedom S and T , and (ii) eight Majorana fields $\chi_{\mathcal{A}\pm}$. Our J_\perp term, for example, takes the form $iJ_\perp d_- \chi_{sf+}(0)$, which couples the local spin Majorana (d_-) and the conduction electrons’ spin-flavor degree of freedom χ_{sf+} .

B. Toulouse limit of the SO(5) fixed point

The PH-symmetric model which flows to the SO(5)-symmetric point is obtained by combining the terms $\mathcal{H}_{\text{SO}(5)}^* = H_0 + H_J + H_{V_z} + H_{Q_\perp}$. At the Toulouse point, it is given by

$$\mathcal{H}_{\text{SO}(5)}^* = H_0 + iJ_\perp d_- \chi_+ - 2Q_\perp^z a_- \chi_+ d_- d_+ - 2iQ_\perp^+ d_+ a_-, \quad (36)$$

where $\chi_\pm \equiv \chi_{sf\pm}(x=0)$.

We now consider the Hamiltonian Eq. (36) from a RG perspective. With respect to the free-fermion fixed point H_0 , bulk fermions such as χ_\pm have scaling dimension $\Delta_\chi = 1/2$ (with correlation function decaying as $1/t^{2\Delta_\chi}$), while local Majoranas have scaling dimension zero. Boundary operators of scaling dimension ≤ 1 are relevant.

First, the J_\perp term resulting from the spin-flip interaction is relevant ($\Delta_{J_\perp} = 1/2$). At energies lower than the Kondo temperature $\sim J_\perp^2$ the Majorana d_- gets “absorbed” into the Majorana bulk field χ_+ , resulting in [60]

$$d_- \approx \frac{\chi_+}{\sqrt{T_K}}. \quad (37)$$

Thus d_- picks up a scaling dimension $1/2$ near the Kondo fixed point.

The Q_\perp^+ operator of dimension zero gaps out the d_+ and a_- operators. The product $ia_- d_+$ obtains then an expectation value. Replacing this operator in Q_\perp^z by a constant results in a term of the same form as $\chi_+ d_-$, which can be used to redefine $J_\perp \rightarrow J'_\perp$. We end up with a Majorana fixed-point Hamiltonian, whose couplings are represented visually in the figure in column 1 of Table II,

$$\mathcal{H}_{\text{SO}(5)}^* \rightarrow H_0 + iJ'_\perp d_- \chi_+ - 2iQ_\perp^+ d_+ a_-. \quad (38)$$

1. Perturbations

Next, we add symmetry-breaking perturbation to the Toulouse fixed-point Hamiltonian. Channel symmetry breaking represented by the J_- term in Eq. (7) takes the form

$$H_{J_-} = iJ_- d_- d_+ \psi_{sf}^\dagger \psi_{sf} - iJ_- d_+ \chi_-. \quad (39)$$

As will be discussed in Sec. IV, both terms are irrelevant since d_+ is already gapped out. The least irrelevant (second) term couples d_+ to χ_- , in addition to the couplings of Eq. (38) (see figure in column 3 of Table II).

Additional key perturbations emerge from breaking PH symmetry. First, those include V_\perp and Q_z :

$$\begin{aligned} H_{V_\perp, Q_z} &= -iV_\perp a_+ \chi_- + 2Q_z (a_- a_+) d_+ \chi_- \\ &- Q_z (a_- a_+) d_- d_+ \psi_{sf}^\dagger \psi_{sf}. \end{aligned} \quad (40)$$

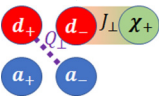
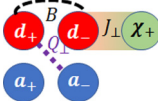
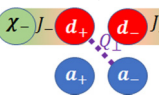
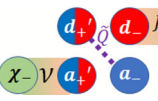
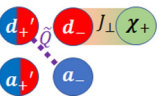
As before, we can use the finite expectation value of $id_+ a_-$ to see that the second term (Q_z) simply renormalizes the first term (V_\perp). Similarly the third term in the second line is less relevant than the first two.

Second, one has the flavor field perturbation

$$H_{B_f} = iB_f' a_- a_+. \quad (41)$$

In addition to the bare flavor field $E_c(1 - 2n_g)$, this operator corrects the coefficient of B_f due to higher-order terms including ϕ_- . We thus consider this as a renormalization of n_g .

TABLE II. A summary of characteristics of different states of our spin-flavor model (rows and columns correspond to different observables and states, respectively). The system's states are as follows (from left to right): (1) SO(5) symmetry with both PH symmetry ($n_g = \frac{1}{2}$, $\eta = 0$) and LR symmetry (t_L and t_B tuned such that $J_- = 0$). (2) Broken spin symmetry with an external magnetic field B . (3) Channel asymmetry, where the tunneling couplings t_L, t_B are detuned such that $J_- \neq 0$. (4) PH breaking I: Upon adding generic PH asymmetry ($\epsilon_d/U \neq -1/2$, $n_g \neq 1/2$), the system becomes a FL. (5) PH breaking II: PH-symmetry-breaking parameters are fine tuned such that a NFL is restored. The rows, from top to bottom, stand for $T \rightarrow 0$ impurity's entropy, spin susceptibility, flavor susceptibility, and conductance between source and drain leads. The final row illustrates the couplings between the local and bulk Majorana fermions. The red, blue, and green balls represent local-spin, local-flavor, and bulk Majorana fermions, respectively. Dashed lines connect local Majoranas, while reddish strips represent couplings of a local Majoranas to a Majorana field. Mixed-color balls imply that a Majorana basis rotation was performed.

	(1) SO(5) symmetry	(2) Magnetic field, B	(3) Channel asymmetry, J_-	(4) PH symmetry breaking I (B_f, V_\perp)	(5) PH symmetry breaking II, NFL line
S_{imp}	$\frac{1}{2} \log 2$	$\frac{1}{2} \log 2$	$\frac{1}{2} \log 2$	0	$\frac{1}{2} \log 2$
χ_s	ω	ω	ω	ω	const
χ_f	ω	const	const	ω	const
$\delta G(\omega)$	$(\frac{\omega}{T_k})^{\frac{3}{2}}$	$(\frac{\omega}{T_k})^{\frac{1}{2}}$	$(\frac{\omega}{T_k})^{\frac{1}{2}}$	$(\frac{\omega}{T_k})$	$(\frac{\omega}{T_k})^{\frac{1}{2}}$
Majorana coupling scheme					

2. Deviations from the Toulouse point

Generically there are deviations from the Toulouse point condition, Eq. (28), resulting in terms of the form

$$\begin{aligned} \delta H_s &= i(J_z - v_F)d_- d_+ \psi_s^\dagger \psi_s, \\ \delta H_f &= i(V_z - v_F)a_- a_+ \psi_f^\dagger \psi_f. \end{aligned} \quad (42)$$

As we see in the following section, these terms are important for the analysis of the effect of generic perturbations on transport and thermodynamic properties of the system.

IV. NFL SO(5) FIXED POINT

The PH-symmetric NFL SO(5) point is located at $n_g = 1/2$ and $\eta = 0$, where in addition a channel symmetry is imposed by tuning the tunnelings t_L, t_B so that $J_- = 0$. Then the effective Hamiltonian is given by Eq. (38). As summarized in column 1 of Table II, in this section we present the thermodynamic behavior in terms of entropy, spin and flavor susceptibilities, and the conductance at the SO(5) point.

A. Entropy

Looking at $\mathcal{H}_{\text{SO}(5)}^*$ in Eq. (38), the Hamiltonian with both channel and PH symmetries, we see that out of the four local Majoranas, only a_+ is decoupled (see schematic illustration in column 1 in Table II).

Similar to the spin-2CK case with an unpaired Majorana [56], this explains the fractional entropy of $\frac{1}{2} \log 2$, observed for $T \rightarrow 0$ in either one of the NRG plots in the first row in Fig. 4 where the perturbations are sent to zero [LR symmetry, $\lambda = 1$, in Fig. 4(a); zero magnetic field, $B = 0$, in Fig. 4(d); or PH symmetry, $\eta = \epsilon_d + U/2 = 0$, in Fig. 4(g)]. In contrast to the spin-2CK model, in our case the free Majorana is assigned to the flavor degree of freedom T .

B. Spin and flavor susceptibilities

Consider the spin susceptibility $\chi_s(t) = \langle S^z(t)S^z(0) \rangle$. The impurity's spin can be written in the Majorana language as $S^z = d^\dagger d - \frac{1}{2} = id_- d_+$ using Eq. (35). From Eq. (37) we then obtain

$$\chi_s(t) \propto \frac{1}{T_k} \langle \chi_+(t)\chi_+(0) \rangle \langle d_+(t)d_+(0) \rangle. \quad (43)$$

For the dimension-1/2 fermion field χ_+ , we have $\langle \chi_+(t)\chi_+(0) \rangle \propto \frac{1}{t}$. We now study the behavior of $\langle d_+(t)d_+(0) \rangle$.

For comparison, in the spin-2CK model the Majorana d_+ is decoupled and thus has no dynamics, in which case $\langle d_+(t)d_+(0) \rangle = 1/4$ and $\chi_s^{\text{spin-2CK}}(t) \propto \frac{1}{t}$; Fourier transforming, $\chi_s^{\text{spin-2CK}}(\omega) \propto \text{const}$. In other words, the impurity spin operator admits a low energy expansion in terms of a dimension-1/2 field,

$$S_{\text{spin-2CK}}^z \sim \frac{i}{\sqrt{T_k}} \chi_+ d_+ \quad (\text{scaling dimension } 1/2). \quad (44)$$

In our spin-flavor Kondo model, to find $\langle d_+(t)d_+(0) \rangle$ we recall that d_+ is gapped out along with a_- by the Q_\perp^\dagger term in Eq. (38). This relevant term separates the Hilbert space into low-energy and high-energy subspaces, with energy difference $2Q_\perp^\dagger$, which are the $\pm 1/2$ eigenspaces of $id_+ a_-$. Equivalently we define a complex fermion $f = \frac{1}{\sqrt{2}}(a_- + id_+)$, so that $f^\dagger f = \frac{1}{2} + ia_- d_+$ and $d_+ = \frac{f-f^\dagger}{\sqrt{2i}}$. Namely, $H_{Q_\perp} = -2iQ_\perp^\dagger d_+ a_- = 2Q_\perp^\dagger (f^\dagger f - \frac{1}{2})$. The ground-state subspace $ia_- d_+ = -1/2$ corresponds to $f^\dagger f = 0$, and the excited subspace $ia_- d_+ = 1/2$ to $f^\dagger f = 1$. We define projectors into these subspaces,

$$\mathcal{P}_0 = 1 - f^\dagger f, \quad \mathcal{P}_1 = f^\dagger f. \quad (45)$$

The operators f^\dagger (f) appearing in S^z bridge the low- and high-energy subspaces. Therefore, $\mathcal{P}_0 S^z \mathcal{P}_0 = \mathcal{P}_1 S^z \mathcal{P}_1 = 0$, meaning that $\langle d_+(t)d_+(0) \rangle$ strongly oscillates as $e^{i2Q_\perp^\dagger t}$.

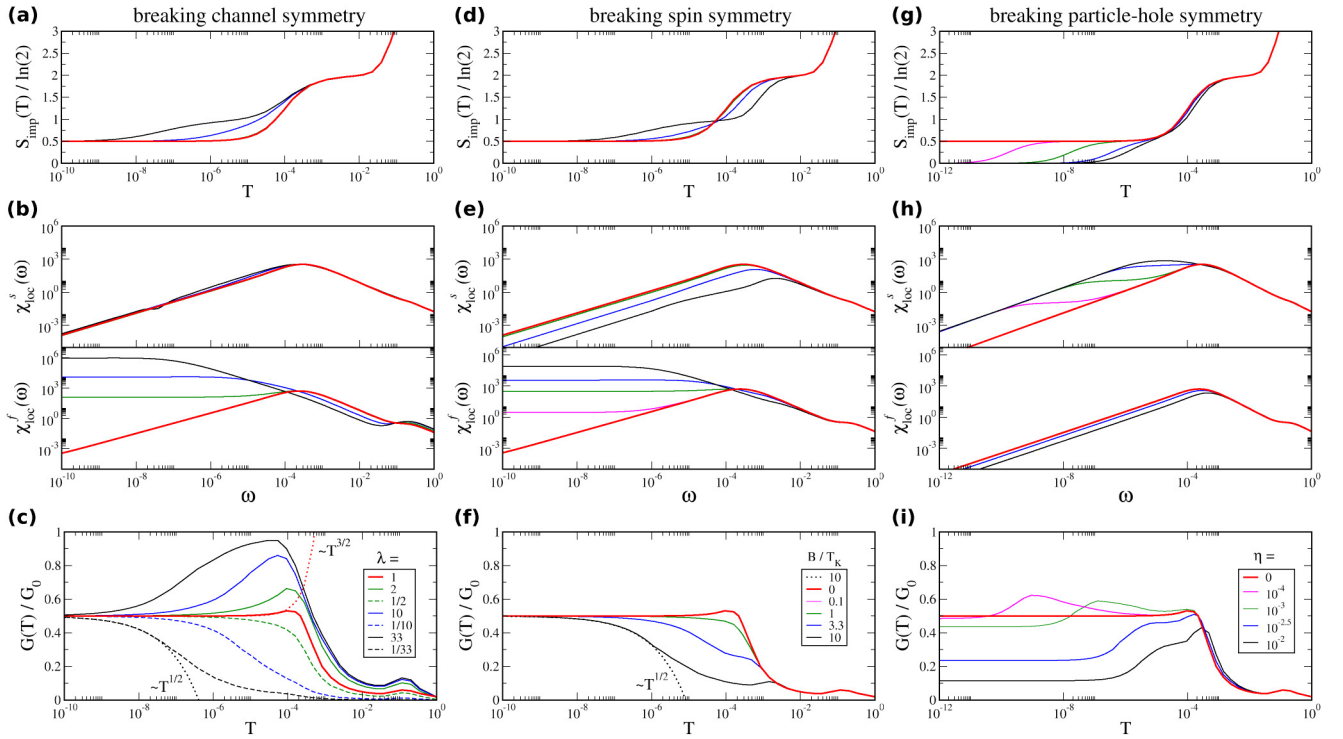


FIG. 4. NRG results for the ALS model with different perturbations. Different columns stand for different perturbations: column 1, channel asymmetry; column 2, magnetic field $B \neq 0$; column 3, particle-hole-symmetry breaking $\eta \neq 0$. Different rows stand for different observables: row 1, the impurity's entropy; row 2, the spin and flavor susceptibilities; and row 3, conductance. The LR asymmetry λ is defined as $\lambda = \xi^2 t_L^2 / t_B^2$ where ξ is found numerically such that at $t_B = \xi t_L$ the system displays LR symmetry; we vary λ for fixed $t_B^2(1 + \lambda) = 0.02$. In our NRG calculations we measure energy in units of the bandwidth $D = 1$, setting $E_c = 0.1$; for further details see Ref. [49]. The dotted curves in (c) and (f) are power-law fits; see discussions in Secs. IV C and V B.

Similar to a SW transformation, to obtain the leading operator expansion of S^z at the spin-flavor fixed point, we perform perturbation theory in off-diagonal operators with respect to projectors \mathcal{P}_{01} . We define for any operator $\mathcal{O}_{ij} = \mathcal{P}_i \mathcal{O} \mathcal{P}_j$, including for the Hamiltonian $H_{ij} = \mathcal{P}_i H \mathcal{P}_j$. For the fixed-point Hamiltonian Eq. (38), off-diagonal terms H_{01}, H_{10} do exist and originate from deviations from the Toulouse point [see $\delta H_{s,f}$ in Eq. (42)], since they include only one Majorana out of the pair d_+, a_- . To second order in off-diagonal operators, we find that the expectation value of any off-diagonal operator (like S^z) takes the form $\langle \mathcal{O} \rangle = \langle \mathcal{O}_{01} (E - H_{11})^{-1} H_{10} + H_{10} (E - H_{11})^{-1} \mathcal{O}_{10} \rangle$, where E here is the ground-state energy. Using $E - H_{11} \cong -2Q_{\perp}^{\pm}$ for the excitation energy, we see that off-diagonal operators do obtain an effective operator form acting in the ground-state subspace,

$$\mathcal{O}_{00,\text{eff}} = \frac{1}{-2Q_{\perp}^{\pm}} (\mathcal{O}_{01} H_{10} + H_{10} \mathcal{O}_{10}). \quad (46)$$

Thus, we obtain

$$S_{\text{spin-flavor}}^z \sim -\frac{J_z - v_F}{4Q_{\perp}^{\pm}} \psi_s^{\dagger} \psi_s - i \frac{V_z - v_F}{2Q_{\perp}^{\pm} \sqrt{T_K}} \chi_+ \psi_f^{\dagger} \psi_f a_+ + \dots \quad (47)$$

The first term has a scaling dimension 1, and coincides with the spin current [61]. This term appears in any FL state. The second term has scaling dimension 3/2 and the dots stand for less relevant terms.

From the first leading term, the spin susceptibility decays as $\frac{1}{T^2}$. In frequency space this becomes $\chi_s(\omega) \sim \omega$, as displayed column 1, row 2, in Table II, matching the linear behavior of the NRG calculated spin susceptibility in Fig. 4.

The flavor susceptibility $\chi_f(t) = \langle T^z(t) T^z(0) \rangle$ can be dealt with in a similar manner using its fermionic form $T^z = a^{\dagger} a - \frac{1}{2} = i a_- a_+$. The leading term is

$$T_{\text{spin-flavor}}^z \sim -\frac{V_z - v_F}{4Q_{\perp}^{\pm}} \psi_f^{\dagger} \psi_f + \dots, \quad (48)$$

which has scaling dimension 1 (with an additional dimension-3/2 operator originating from $J_z - v_F$), leading to a FL-like behavior $\chi_f(t) \sim \frac{1}{t^2}$, or $\chi_f(\omega) \sim \omega$, matching our NRG results in Fig. 4.

C. Leading irrelevant operator and conductance

The temperature dependence of the conductance for the multichannel Kondo effect probes the leading irrelevant (boundary) operator at the nontrivial fixed point [13,62]. From scaling analysis, a boundary perturbation of dimension Δ yields to first order a temperature dependence of the conductance of the form $\delta G \sim T^{\Delta-1}$.

In the spin-2CK state there exists an anomalous operator of dimension $\Delta = 3/2$ originally found by CFT [62], leading to the experimentally observed $\delta G \sim T^{1/2}$ scaling of the conductance [10]. We can identify this dimension-3/2 operator in the Majorana fermion language: In the spin-2CK case, with

the Q_{\perp}^{\perp} term absent and hence d_{+} being a free Majorana, δH_s in Eq. (42) becomes

$$(\delta H_s)^{(\text{spin-2CK})} \sim \frac{i(J_z - v_F)}{\sqrt{T_K}} (\chi_{+} \psi_s^{\dagger} \psi_s) d_{+} \quad (\text{scaling dimension } 3/2). \quad (49)$$

As discussed in Sec. IV B, in the spin-flavor model δH_s does not commute with Q_{\perp}^{\perp} and is off-diagonal in our two-subspace decomposition, Eq. (45). The leading irrelevant operator can be obtained from second-order perturbation theory in off-diagonal operators,

$$H_{00,\text{eff}} = H_{01}(E - H_{11})^{-1}H_{10}. \quad (50)$$

To obtain a nontrivial operator, this time we have to combine δH_s and δH_f to obtain

$$\delta H_{\text{irr}} = -i \frac{(J_z - v_F)(V_z - v_F)}{2Q_{\perp}^{\perp} \sqrt{T_K}} (\chi_{+} \psi_s^{\dagger} \psi_s \psi_f^{\dagger} \psi_f) a_{+} \quad (\text{scaling dimension } 5/2). \quad (51)$$

We see that the leading irrelevant operator involves both spin and flavor degrees of freedom and has a total scaling dimension of 5/2. It leads to a conductance scaling $\delta G \sim T^{\frac{3}{2}}$, as observed in Figs. 4(c), 4(f), and 4(i) (see graphs for unperturbed cases).

V. PERTURBATIONS

Having analyzed the effective Hamiltonian and the resulting physical properties at the SO(5) fixed point, as summarized in the first column of Table II, we now discuss perturbations summarized in the remaining columns of Table II.

A. Magnetic field

In the middle column of Fig. 4 we show NRG results for the entropy, susceptibilities, and conductance in the presence of a magnetic field B . We can see that a residual $\frac{1}{2} \log 2$ entropy persists as $T \rightarrow 0$, implying a NFL state. We also observe a $\log 2$ intermediate temperature plateau, indicating the quenching of the spin degeneracy at $T < B$, followed by a NFL behavior. While neither the $\frac{1}{2} \log 2$ entropy at $T \rightarrow 0$ nor the ω scaling of the spin susceptibility are affected by B , the flavor susceptibility χ_f is no longer linear in ω , and becomes a constant instead.

These behaviors can be accounted for within the Majorana fermion framework. The magnetic field term $-iBd_{+}d_{-}$ can be incorporated into the fixed-point Hamiltonian (38). It can be readily combined with the $-2iQ_{\perp}^{\perp}d_{+}a_{-}$ term by a Majorana rotation,

$$\begin{pmatrix} a'_{-} \\ d'_{-} \end{pmatrix} = \begin{pmatrix} \cos \alpha_B & \sin \alpha_B \\ -\sin \alpha_B & \cos \alpha_B \end{pmatrix} \begin{pmatrix} a_{-} \\ d_{-} \end{pmatrix}, \quad (52)$$

where $\sin \alpha_B = \frac{B}{\sqrt{(2Q_{\perp}^{\perp})^2 + B^2}}$, yielding

$$\begin{aligned} \mathcal{H}_{\text{SO}(5)}^* - iBd_{+}d_{-} &= H_0 + iJ_{\perp}^{\perp}(\cos(\alpha_B)d'_{-} + \sin(\alpha_B)a'_{-})\chi_{+} \\ &\quad - i2Q'_{\perp}d_{+}a'_{-}, \end{aligned} \quad (53)$$

where $Q' = \sqrt{(Q_{\perp}^{\perp})^2 + (B/2)^2}$. We first notice that a_{+} remains free (see scheme in column 2 of Table II), supporting the observed $\frac{1}{2} \log 2$ entropy at $T \rightarrow 0$. Although the Majorana rotation, Eq. (52), maintains the system in a NFL state, it does modify certain correlation functions.

The operator expansion of the impurity spin operator S^z , to leading order in B , remains as in Eq. (47), governed by the dimension-1 operator $\psi_s^{\dagger} \psi_s$, so that the spin susceptibility remains FL-like.

On the other hand, the flavor impurity operator $T^z = ia_{-}a_{+}$ now obtains a diagonal component in terms of the rotated projectors $\mathcal{P}_{0,1}$, which are defined as in Eq. (45), but in terms of the rotated Majorana pair (d_{+}, a'_{-}) instead of (d_{+}, a_{-}) . In the expression $T^z = ia_{-}a_{+}$, the Majorana a_{+} is free, and $a_{-} = \cos \alpha_B a'_{-} - \sin \alpha_B d'_{-}$ contains a component $\propto \sin \alpha_B \propto B/(2Q_{\perp}^{\perp})$ which is diagonal in the low- and high-energy subspaces associated with the Q' term. Thus,

$$(T_{(+B)}^z)_{00} \sim -i \frac{B}{2Q_{\perp}^{\perp} \sqrt{T_K}} \chi_{+} a_{+} \quad (\text{scaling dimension } 1/2). \quad (54)$$

Hence, the magnetic field causes the flavor operator to scale like the fermion field χ_{+} , and acquire a scaling dimension 1/2. As a result $\chi_f(t) \sim \frac{1}{t}$ ($\chi_f(\omega) \sim \text{const}$).

To address the effect of the magnetic field on the conductance, we identify the leading irrelevant operator. In the absence of B the leading operator of dimension 5/2 in Eq. (51) resulted from combining δH_s and δH_f , each of which individually bridges the low- and high-energy sectors of Q_{\perp}^{\perp} . However, in the presence of B and the associated Majorana rotation, δH_f alone contributes to the leading irrelevant operator

$$\delta H_{\text{irr}}^{(+B)} = (\delta H_f)_{00} = -i(V_z - v_F) \frac{B}{2Q_{\perp}^{\perp} \sqrt{T_K}} (\chi_{+} \psi_f^{\dagger} \psi_f) a_{+}, \quad (55)$$

which has scaling dimension $\Delta = 3/2$. Thus, the conductance scaling is modified into a $\delta G \sim T^{1/2}$ form. This is indeed observed in Fig. 4(f).

B. Breaking channel symmetry

We now consider broken LR symmetry while still preserving PH symmetry. Among the list of operators in Table I, this case includes J_{-} and V_z^{-} . The most relevant term is $\delta H_{-} = -iJ_{-}d_{+}\chi_{-}$ [see Eq. (39)]. This extra coupling between χ_{-} and d_{+} , shown in Table II, column 3, still leaves the a_{+} Majorana decoupled, implying a fixed point with $\frac{1}{2} \log 2$ entropy.

To determine the low-energy behavior of the spin susceptibility, we look at the operator expansion of S^z , which in the absence of J_{-} is given by the dimension-1 operator $\psi_s^{\dagger} \psi_s$ in Eq. (47). The leading-order expansion of $S^z = id_{-}d_{+}$ is obtained from Eq. (46) where $H_{10}, H_{01} \propto J_{-}$. However, due to anticommutation relations, Eq. (46) yields a vanishing contribution in this case. Hence the FL-like behavior of χ_s persists.

As for the flavor susceptibility, the flavor impurity operator $T^z = ia_{-}a_{+}$ now combines with J_{-} according to Eq. (46) to

yield a dimension-1/2 operator of the form

$$T^z \sim -i \frac{J_-}{2Q_\perp} \chi_{-a_+}. \quad (56)$$

Namely, the flavor susceptibility acquires NFL behavior at low energy.

Finally, the leading irrelevant operator stems from δH_f combined with H_- in Eq. (50). It yields a dimension-3/2 operator

$$\delta H_{\text{irr}} \sim -i \frac{J_-(V_z - v_F)}{2Q_\perp} \chi_-(\psi_f^\dagger \psi_f) a_+, \quad (57)$$

which leads to a $T^{1/2}$ scaling of the conductance as confirmed in Fig. 4(c).

These low-energy limits of the entropy, spin and flavor susceptibilities, and conductance are summarized in Table II, column 3.

We now further discuss these results from our NRG simulations. In Fig. 4(a) we see the impurity entropy as a function of temperature for $(n_g, \eta) = (\frac{1}{2}, 0)$ and for various ratios between the left and right tunnelings $\lambda \propto t_L^2/t_B^2$. While the $T = 0$ fixed-point entropy remains $\frac{1}{2} \log 2$ in all cases, channel asymmetry changes the way in which the entropy goes to its fixed-point value. As asymmetry grows, two successive crossovers appear: one from $\log(4)$ to $\log(2)$ on a scale T_K^1 , and a second from $\log(2)$ to $\log(2)/2$ at a scale $T_K^2 < T_K^1$. This is in contrast to the symmetric case which shows a single drop from $\log(4)$ to $\log(2)/2$. In the strongly asymmetric limit one can associate [63,64] the first drop with a 1CK screening of the spin degree of freedom, while the $\frac{1}{2} \log 2$ drop is a nontrivial signature of a 2CK partial screening and relates to the flavor degree of freedom. This claim is supported by our NRG calculation of the magnetic susceptibility in Fig. 4(b), where only one crossover is observed at T_K^1 . This indicates that the second crossover at T_K^2 for large asymmetry occurs in the flavor sector.

C. Breaking particle-hole symmetry

PH symmetry is broken away from the point $(n_g, \eta) = (\frac{1}{2}, 0)$. As can be seen in our NRG calculations in the right column of Fig. 4, in this case the NFL is destabilized, with a drop of the entropy to zero in Fig. 4(g). Notice that the flavor field which is turned on for $n_g \neq 0$, breaks PH symmetry as well as LR symmetry. Thus we should consider all the corresponding terms in Table I ($V_\perp, Q_z; \phi; J_-, Q_z^-, V_z^-, \phi^-; B_f$). We focus on a subset of these perturbations which leads to a relevant instability of the SO(5) NFL state.

As in Sec. V A, we begin with incorporating the Majorana-Majorana flavor coupling, $iB_f a_- a_+$, into the fixed-point Hamiltonian. It can be combined with the $-2iQ_\perp^\dagger d_+ a_-$ term by another Majorana rotation,

$$\begin{pmatrix} \tilde{d}_+ \\ \tilde{a}_+ \end{pmatrix} = \begin{pmatrix} \cos \alpha_{B_f} & \sin \alpha_{B_f} \\ -\sin \alpha_{B_f} & \cos \alpha_{B_f} \end{pmatrix} \begin{pmatrix} d_+ \\ a_+ \end{pmatrix}, \quad (58)$$

where $\sin \alpha_{B_f} = \frac{B_f}{\sqrt{(2Q_\perp^\dagger)^2 + B_f^2}}$, yielding

$$\mathcal{H}_{\text{SO}(5)}^* - iB_f a_+ a_- = H_0 + iJ_\perp d_- \chi_+ - i2\tilde{Q}_\perp^\dagger \tilde{d}_+ \tilde{a}_-, \quad (59)$$

where $\tilde{Q} = \sqrt{(Q_\perp^\dagger)^2 + (B_f/2)^2}$. We first notice that instead of a_+ , at this stage \tilde{a}_+ is free (see Majorana scheme in column 4 of Table II). However, adding generic perturbations that break PH and LR symmetry, no Majorana remains free. We identify three perturbations, V_\perp, Q_z , and J_- , that when turned on, take the form of a dimension-1/2 coupling $i\tilde{a}_+ \chi_-$. Explicitly, keeping only relevant operators in $H_{V_\perp, Q_z} + \delta H_-$ in Eqs. (39) and (40), we find

$$\begin{aligned} H_{V_\perp, Q_z} + \delta H_- &\rightarrow -i\mathcal{V} \tilde{a}_+ \chi_-, \\ \mathcal{V} &= \cos \alpha_{B_f} (V_\perp + Q_z) - \sin \alpha_{B_f} J_-. \end{aligned} \quad (60)$$

Due to the coupling \mathcal{V} which is generically finite when PH symmetry is broken, the so-far-free Majorana \tilde{a}_+ is coupled to the conduction electrons; hence the residual entropy is quenched, and the system turns into a FL [see Fig. 4(g)]. In this case, resorting to the methods developed above, one can show that the system shows no anomalous NFL behavior; i.e., the impurity spin and flavor operators acquire scaling dimension 1, and the leading irrelevant operator has scaling dimension 2. This is summarized in column 4 of Table II. However, as we discuss next, the NFL state can be recovered even in the PH- and LR-symmetry-broken phase, upon fine tuning.

VI. EMERGENCE OF NFL LINE FROM SO(5) POINT IN THE (n_g, η) PHASE DIAGRAM

The coupling constant \mathcal{V} in Eq. (60) depends on the tunneling amplitudes of the lead-dot-box model through the explicit forms of the various couplings, obtained through the SW transformation in Appendix A. The condition

$$\mathcal{V}(J_-, V_\perp, Q_z, B_f) = 0 \quad (\text{NFL}) \quad (61)$$

implies that the system is fine tuned to a NFL state with a residual $\frac{1}{2} \log 2$ entropy.

For a given t_L/t_B one can solve the equation $\mathcal{V}(\epsilon_d, U, E_c, t_L, t_B) = 0$ for n_g as a function of η . The resulting function is a NFL curve in the (n_g, η) phase diagram which approaches the SO(5) point. This is plotted in Fig. 5, where we solved Eq. (61), $\mathcal{V}(\epsilon_d, U, E_c, t_L^{\text{NRG}} \alpha, t_B^{\text{NRG}} \alpha) = 0$ for different tunneling ratios. The cutoff scheme in NRG is different, allowing one fitting parameter α which is found to give optimal fitting for $\alpha \cong 0.11$. We see that these curves qualitatively match the observed NRG NFL lines in the proximity of the $n_g = 0.5, \eta = 0$ point. While our NRG results of Ref. [49] extend in the entire (n_g, η) phase diagram, which is periodic in $n_g \rightarrow n_g + 1$ (see Fig. 1 in Ref. [49]), our SW mapping which considered a limited number of charge states is restricted to the vicinity of point $n_g = 1/2$.

While the fit shows the various NFL curves emanating from the SO(5) point with a LR-asymmetry-dependent slope, the Toulouse limit approach is expected only to reproduce reliably the scaling properties (summarized in Table II), but not the detailed dependence on model parameters.

Along the NFL curve, the Majorana \tilde{a}_+ remains decoupled. At the SO(5) point, $B_f = 0$, it coincides with a_+ from the flavor sector [see Eq. (58)]. As B_f increases, the free Majorana tends toward d_+ from the spin sector. This indicates a smooth rotation in the spin and flavor space [46–48].

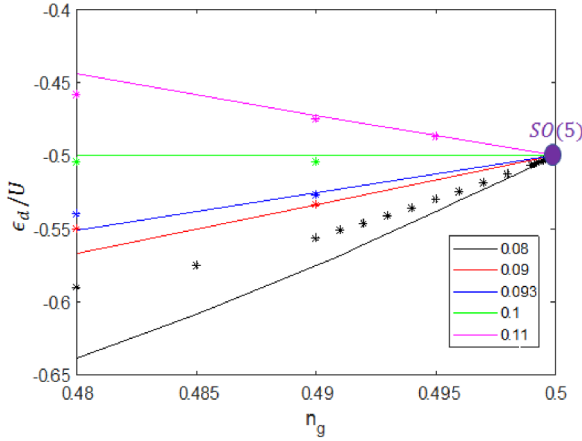


FIG. 5. Numerical solutions of Eq. (61), representing the evolution of the NFL curve in the n_g - ϵ_d plane in the proximity of the $n_g = \frac{1}{2}$ point. These numerical solutions (continuous curves) are qualitatively fitted to NRG results using a single parameter α ; see main text. The caption denotes the values $t_L^{\text{NRG}} = 0.08, 0.09, 0.1, 0.11, 0.092235$ and $t_R^{\text{NRG}} = 0.12$ used in the NRG calculations for the ALS model.

Physical properties

We see that if we deviate from the SO(5) point along a specific direction, the system's NFL nature persists. We then have a free Majorana fermion, \tilde{a}_+ , as illustrated in the scheme in column 5 of Table II. Rather than the SO(5) NFL, we have generically on the NFL line a behavior similar to the spin-2CK NFL state, as implied by the physical signatures discussed next.

Using Eqs. (37) and (58), the spin operator contains the terms $S^z = id_-d_+ = i\frac{\chi_{\pm}}{\sqrt{T_K}}(\cos(\alpha_{B_f})\tilde{d}_+ + \sin(\alpha_{B_f})\tilde{a}_+)$. Keeping only its low-energy component,

$$(S^z)_{00} \sim \frac{1}{\sqrt{T_K}} \sin(\alpha_{B_f}) i\chi_+ \tilde{a}_+. \quad (62)$$

Comparing with Eq. (44) in the spin-2CK case, the spin susceptibility along the NFL curve contains a NFL component $\propto \sin^2(\alpha_{B_f})$ which vanishes at the SO(5) point, $\chi_s(\omega) \propto \text{const} \times \sin^2(\alpha_{B_f}) + \mathcal{O}(\omega)$.

As for the flavor susceptibility, since we generically have a finite J_- operator on the NFL line, we have the same dimension-1/2 operator as in Eq. (56) leading to a NFL flavor susceptibility. Similarly, there is a dimension-3/2 leading irrelevant operator $\propto J_-$ as in Eq. (57).

VII. SUMMARY

We revisited a quantum impurity problem describing a quantum dot device where two channels of electrons interact both with an impurity spin and with an additional ‘‘flavor’’ impurity. Using bosonization and refermionization, we constructed a consistent picture describing the coupling of the impurity degrees of freedom with the conduction electrons, and allowing to compute the various observables. Our field theory results are consistent with our numerical renormalization group calculations, and with a non-Fermi liquid fixed point exhibiting SO(5) emergent symmetry.

So far, it was believed that the device displays exotic two-channel Kondo behavior upon tuning the channel asymmetry to zero. Our study shows that the NFL behavior is much more robust and extends to generic values of the channel asymmetry, upon tuning of the quantum dot level position. As demonstrated here in great detail, we reached this understanding from the high-symmetry fixed point. Using NRG, as already demonstrated in Ref. [49], we found how this SO(5) fixed point connects in the phase diagram to the more conventional spin-two-channel Kondo state. Our predictions within the system's complex phase diagram can be tested experimentally, in terms of conductance [10,11] and also more recent entropy measurements [65–67].

ACKNOWLEDGMENTS

A.K.M. and E.S. acknowledge the Stewart Blusson Quantum Matter Institute (UBC) for travel support. A.K.M. acknowledges funding from the Irish Research Council Laureate Awards 2017/2018 through Grant No. IRCLA/2017/169. I.A. acknowledges financial support from NSERC Canada Discovery Grant No. 0433-2016. E.S. acknowledges support from ARO (Grant No. W911NF-20-1-0013), the Israel Science Foundation Grant No. 154/19, and US-Israel Binational Science Foundation (Grant No. 2016255).

APPENDIX A: SCHRIEFFER-WOLFF (SW) TRANSFORMATION

We derive the effective Hamiltonian (1) among the various additional interaction terms summarized in Table I, starting from the lead-dot-box model. The system is initially either in the $(N_0, N_0 + 1)$ or $(N_0 + 1, N_0)$ charge state of the lead and box, with one electron (with spin up or down) in the small dot. To second order in the tunneling amplitude, depending on the initial state, the system visits one of the four intermediate states depicted in Fig. 6. As long as the lead and box are equally treated as left and right reservoirs, the left and right sides of Fig. 6 are related by left-right transformation. Here, solid and dashed arrows represent the first and second tunneling events, respectively. For later use we detail the associated energies at zero tunneling. The energy is obtained from Eqs. (2) and (3), $E = E_c(N_B - N_0 - n_g)^2 + \epsilon_d n_d + U n_{\uparrow} n_{\downarrow}$. For the two initial states, $E^{(N_0, N_0+1)} = E_c(1 - n_g)^2 + \epsilon_d$ and $E^{(N_0+1, N_0)} = E_c n_g^2 + \epsilon_d$. We assume without loss of generality that $n_g \leq 1/2$, so the ground-state energy is $E_{GS} = E^{(N_0+1, N_0)}$. For example, the energy of the first intermediate state in Fig. 6, in which an electron tunnels from the small dot to the box, is $\epsilon_1^+ = E_c(2 - n_g)^2$, while $\epsilon_1^- = E_c n_g^2$. We define $E_j^{\pm} \equiv E_{GS} - \epsilon_j^{\pm}$ ($j = 1, 2, 3, 4$), which are given explicitly by

$$\begin{aligned} E_1^+ &= \epsilon_d + 4E_c(n_g - 1), \\ E_2^+ &= \epsilon_d + E_c(2n_g - 1) = E_2^-, \\ E_3^+ &= -\epsilon_d + E_c(2n_g - 1) - U, \\ E_4^+ &= -\epsilon_d - U = E_4^-, \\ E_1^- &= \epsilon_d, \\ E_3^- &= -\epsilon_d - E_c(2n_g + 1) - U. \end{aligned} \quad (\text{A1})$$

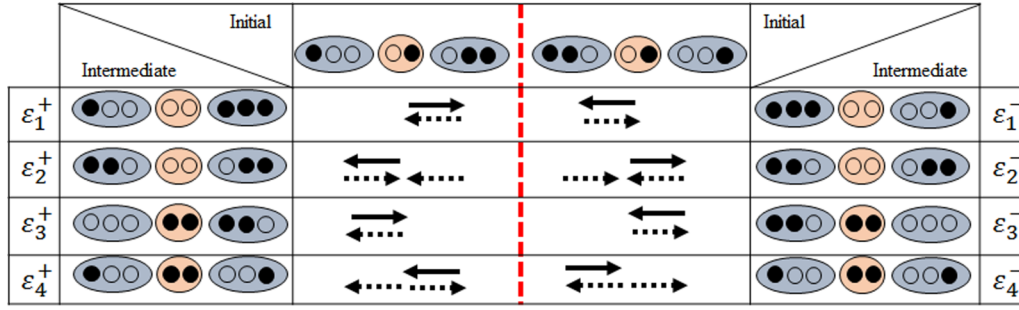


FIG. 6. Schematic representation of virtual transitions considered in our SW expansion. The two middle columns of the first row represent the two possible initial charge states $(N_0, N_0 + 1)$ on the left and $(N_0 + 1, N_0)$ on the right. The red circle represents the dot, the blue ellipse represents the box and/or leads, and the small open or solid circles indicate occupancy by electrons. The two outer columns show the intermediate states. Solid arrows represent the direction in which electrons hop to reach the intermediate state, and dashed arrows represent the electronic hopping yielding final state. The intermediate states' energy is denoted by ε_i^\pm . For instance, the process that begins with an initial state of $(N_0 + 1, N_0)$ becomes $(N_0 + 1, N_0 - 1)$ after an electron hops from the box to the dot, through the intermediate state of energy ε_3^- .

To perform perturbation theory in the hybridization, we start from the ALS model,

$$H_{\text{ALS}} = \sum_{\alpha=L,R} \sum_{k,\sigma} \epsilon_k \psi_{k\alpha\sigma}^\dagger \psi_{k\alpha\sigma} + E_c (T_B^z - N_0 - n_g)^2 + H_d + \sum_{k\alpha\sigma} t_\alpha (d_\sigma^\dagger \psi_{k\alpha\sigma} T_\alpha^- + \text{H.c.}), \quad (\text{A2})$$

where in comparison to Eq. (5), we added another pseudospin T operator to the lead for convenience. Denoting the lead as the left (L) reservoir, and the box as the right (R) reservoir, we thus have two pseudospin operators $T_{L,R}$, whose z component measures whether the corresponding reservoir is in the $N_0 + 1$ state ($T_\alpha = 1/2$) or N_0 state ($T_\alpha = -1/2$) and T^+ increases the charge from N_0 to $N_0 + 1$.

Treating the tunneling operators as a perturbation, $H_{\text{ALS}} = \mathcal{H}_0 + H_{\text{hyb}}$ where $\mathcal{H}_0 = H_0 + H_B + H_d$, to second order the effective Hamiltonian is

$$\delta H_{\text{eff}} = H_{\text{hyb}} \frac{1}{E - \mathcal{H}_0} H_{\text{hyb}}, \quad (\text{A3})$$

where $E = E_{\text{GS}}$, giving

$$\delta H_{\text{eff}} = \sum_{k,k',\alpha,\beta,\sigma,\sigma'} t_\alpha t_\beta \left(d_\alpha^\dagger c_{k\alpha\sigma} T_\alpha^- \frac{1}{E - \mathcal{H}_0} T_\beta^+ c_{k'\beta\sigma'}^\dagger d_{\sigma'} + T_\alpha^+ c_{k\alpha\sigma}^\dagger d_\sigma \frac{1}{E - \mathcal{H}_0} d_\sigma^\dagger c_{k'\beta\sigma'} T_\beta^- \right). \quad (\text{A4})$$

The first term corresponds to hole processes with an empty small dot intermediate state (states $\varepsilon_{1,2}^\pm$ in Fig. 6) while the second corresponds to particle processes involving a doubly occupied small dot (states $\varepsilon_{3,4}^\pm$ in Fig. 6). The energy denominator represents (minus) the energy difference between the virtual and initial state as given in Eq. (A1). We now reduce the two pseudospin operators back to a single one representing the pair of states $(N_0, N_0 + 1)$ or $(N_0 + 1, N_0)$, defined as

$$T^+ = T_L^- T_R^+, \quad T^- = T_L^+ T_R^-, \quad T^z = T_R^z = -T_L^z. \quad (\text{A5})$$

We also define projection operators, P_+, P_- , into the $(N_0, N_0 + 1)$, $(N_0 + 1, N_0)$ states, respectively:

$$P_+ = 1/2 + T^z, \quad P_- = 1/2 - T^z. \quad (\text{A6})$$

The effective interactions can be separated as $\delta H_{\text{eff}} = H_+ + H_-$ depending on whether the system starts in the $+$ or $-$ state, each of which contains four terms linked with the processes in Fig. 6. For the $(N_0, N_0 + 1)$ initial state we have

$$H_+ = \left[\sum_{k,k',\sigma,\sigma'} t_R^2 \frac{1}{E_1^+} (d_\sigma^\dagger c_{kR\sigma} T_R^- T_R^+ c_{k'R\sigma'}^\dagger d_{\sigma'}) + \sum_{k,k',\alpha,\sigma,\sigma'} t_L t_\alpha \frac{1}{E_2^+} (d_\sigma^\dagger c_{k\alpha\sigma} T_\alpha^- T_L^+ c_{k'L\sigma'}^\dagger d_{\sigma'}) + \sum_{k,k',\sigma,\sigma'} t_L^2 \frac{1}{E_3^+} (T_L^+ c_{kL\sigma}^\dagger d_\sigma d_\sigma^\dagger c_{k'L\sigma'} T_L^-) + \sum_{k,k',\alpha,\sigma,\sigma'} \frac{t_\alpha t_R}{E_4^+} (T_\alpha^+ c_{k\alpha\sigma}^\dagger d_\sigma d_\sigma^\dagger c_{k'R\sigma'} T_R^-) \right] P_+. \quad (\text{A7})$$

Similarly, from the $(N_0 + 1, N_0)$ state (right side in Fig. 6) we generate the interactions

$$H_- = \left[\sum_{k,k',\sigma,\sigma'} t_L^2 \frac{1}{E_1^-} (d_\sigma^\dagger c_{kL\sigma} T_L^- T_L^+ c_{k'L\sigma'}^\dagger d_{\sigma'}) + \sum_{k,k',\alpha,\sigma,\sigma'} t_R t_\alpha \frac{1}{E_2^-} (d_\sigma^\dagger c_{k\alpha\sigma} T_\alpha^- T_R^+ c_{k'R\sigma'}^\dagger d_{\sigma'}) + \sum_{k,k',\sigma,\sigma'} t_R^2 \frac{1}{E_3^-} (T_R^+ c_{kR\sigma}^\dagger d_\sigma d_\sigma^\dagger c_{k'R\sigma'} T_R^-) + \sum_{\alpha,k,k',\sigma,\sigma'} \frac{t_\alpha t_L}{E_4^-} (T_\alpha^+ c_{k\alpha\sigma}^\dagger d_\sigma d_\sigma^\dagger c_{k'L\sigma'} T_L^-) \right] P_-. \quad (\text{A8})$$

Defining local fermion operators $\psi_{\alpha\sigma} = \sum_k c_{k\alpha\sigma}$ and impurity spin $\vec{S} = d_\sigma^\dagger \frac{\vec{\sigma}_{\alpha\alpha'}}{2} d_{\sigma'}$, the resulting effective Hamiltonian can be written as $\delta H_{\text{eff}} = \sum_i \lambda_i \mathcal{O}_i$, where the local operators \mathcal{O}_i and coupling constants λ_i are listed in Table I. Each operator has a well defined left-right (LR) transformation and PH symmetry.

We separated the coupling constants into (i) a pair of operators that transmit charge from left to right (V_\perp and Q_\perp) containing T^\pm , (ii) four operators which are LR

even (J, V_z, Q_z, ϕ), (iii) LR-odd versions of the former four ($J_-, V_{z-}, Q_{z-}, \phi_-$), and (iv) the flavor field T^z .

Following a tedious but straightforward algebra, the coupling constants can be obtained. The explicit form of the pseudospin-flip operators are

$$\begin{aligned} Q_\perp &= -t_{RtL} \left(\frac{1}{E_2^-} + \frac{1}{E_4^-} \right), \\ V_\perp &= -t_{RtL} \left(\frac{1}{E_2^+} - \frac{1}{E_4^+} \right). \end{aligned} \quad (\text{A9})$$

The four couplings which have a LR-odd version, such as J , can be written as $J = J^L + J^R$ and $J_- = J^L - J^R$, and similarly for V_z, Q_z , and ϕ where

$$\begin{aligned} J^R &= -\frac{t_R^2}{2} \left(\frac{1}{E_1^+} + \frac{1}{E_2^-} + \frac{1}{E_3^-} + \frac{1}{E_4^+} \right), \\ Q_z^R &= \frac{t_R^2}{2} \left[\left(\frac{1}{E_1^+} - \frac{1}{E_2^-} \right) - \left(\frac{1}{E_3^-} - \frac{1}{E_4^+} \right) \right], \\ \phi^R &= -\frac{t_R^2}{8} \left[\left(\frac{1}{E_1^+} + \frac{1}{E_2^-} \right) - \left(\frac{1}{E_3^-} + \frac{1}{E_4^+} \right) \right], \\ V_z^R &= \frac{t_R^2}{4} \left[\left(\frac{1}{E_3^-} - \frac{1}{E_4^+} \right) + \left(\frac{1}{E_1^+} - \frac{1}{E_2^-} \right) \right], \end{aligned}$$

and $J^L, Q_z^L, \phi^L, V_z^L$ are obtained from these expressions by interchanging $E_j^+ \leftrightarrow E_j^-$ and $t_R \leftrightarrow t_L$. Similarly, the flavor field is given by $B^R = t_R^2 \left(\frac{1}{E_1^+} - \frac{1}{E_2^-} \right)$. This term correcting Eq. (8) leads simply to a shift in the definition of n_g .

APPENDIX B: PH TRANSFORMATION OF BOSONIC AND MAJORANA FIELDS

Under the PH transformation Eq. (6), $\psi_{\alpha\uparrow} \rightarrow -i\psi_{\alpha\downarrow}^\dagger$ and $\psi_{\alpha\downarrow} \rightarrow i\psi_{\alpha\uparrow}^\dagger$. Rewriting this in terms of boson fields and Klein factors using Eq. (21), we have

$$\begin{aligned} F_{\alpha\uparrow} e^{-i\phi_{\alpha\uparrow}} &\rightarrow -iF_{\alpha\downarrow}^\dagger e^{i\phi_{\alpha\downarrow}}, \\ F_{\alpha\downarrow} e^{-i\phi_{\alpha\downarrow}} &\rightarrow iF_{\alpha\uparrow}^\dagger e^{i\phi_{\alpha\uparrow}}. \end{aligned} \quad (\text{B1})$$

This transformation rule is consistent with

$$F_{\alpha\uparrow} \rightarrow F_{\alpha\downarrow}^\dagger, \quad F_{\alpha\downarrow} \rightarrow +F_{\alpha\uparrow}^\dagger, \quad (\text{B2})$$

and

$$\phi_{\alpha\uparrow} \rightarrow -\phi_{\alpha\downarrow} + \pi/2, \quad \phi_{\alpha\downarrow} \rightarrow -\phi_{\alpha\uparrow} - \pi/2. \quad (\text{B3})$$

Here we made a choice attaching the minus sign in the PH transformation to the bosons rather than Klein factors.

Moving to the $\mathcal{A} = c, s, f, sf$ bosons using Eq. (24), we have

$$\begin{aligned} \phi_{sf} &\rightarrow \phi_{sf}, \quad \phi_s \rightarrow \phi_s + \pi, \\ \phi_f &\rightarrow -\phi_f, \quad \phi_c \rightarrow -\phi_c. \end{aligned} \quad (\text{B4})$$

The relevant perturbation V_\perp in Table I is PH odd. It adds to the Hamiltonian the perturbation $-iV_\perp a_+ \chi_-$, which consists of the Hermitian operator

$$\epsilon = (a^\dagger + a)(\psi_{sf} - \psi_{sf}^\dagger), \quad (\text{B5})$$

where $a = F_f^\dagger T^-$. (The notation ϵ relates to our CFT solution of the problem [49], where this field belonged to the Ising CFT.) We would like to show that ϵ is PH odd. Explicitly

$$\epsilon = (F_f T^- + F_f^\dagger T^-)(F_{sf} e^{-i\phi_{sf}} + F_{sf}^\dagger e^{i\phi_{sf}}). \quad (\text{B6})$$

Now we perform the PH transformation on the pair of Klein factors,

$$F_{sf}^\dagger F_f^\dagger = F_{1\uparrow}^\dagger F_{2\uparrow}^\dagger \rightarrow F_{1\downarrow} F_{2\downarrow}^\dagger = -F_{2\downarrow}^\dagger F_{1\downarrow} = -F_{sf}^\dagger F_f. \quad (\text{B7})$$

In the last equality we used the relation in Eq. (30) and the unitarity of Klein factors. We conclude that under PH symmetry $F_f \rightarrow -F_f^\dagger$. Combining this with $T^+ \rightarrow T^-$, we see that $\epsilon \rightarrow -\epsilon$.

APPENDIX C: WEAK-COUPPLING RG EQUATIONS AND FLOW TOWARDS THE SO(5) FIXED POINT

Derivation of Eq. (18)

We begin with a derivation of Eq. (18) following the perturbative RG approach [68]. Consider a fixed-point theory described by a set of operators \mathcal{O}_i having scaling dimensions Δ_i , and satisfying the operator product expansion (OPE)

$$\mathcal{O}_i(x)\mathcal{O}_j(y) = \sum_k c_{ijk} \frac{\mathcal{O}_k(y)}{(x-y)^{\Delta_i+\Delta_j-\Delta_k}}. \quad (\text{C1})$$

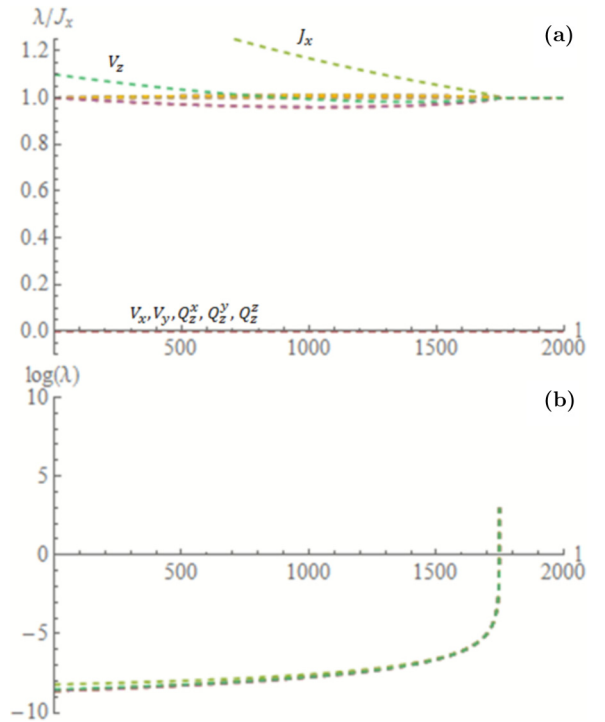


FIG. 7. (a) The value of the couplings (there are 15 of them in total) normalized by J_x , as a function of the RG scale parameter ℓ , for an initial value where all couplings are equal to $u = 0.00018$, except for $J_z = 1.5u$, $V_z = 1.1u$, and $V_x, V_y, Q_z^x, Q_z^y, Q_z^z = 0$. We see that all ratios of couplings flow to unity. (b) For the same RG flow we display on a logarithmic scale the absolute values of the couplings. We see that isotropy is reached together with strong coupling, in which the weak-coupling RG equations become uncontrollable.

Now consider the fixed-point Hamiltonian \mathcal{H}^* perturbed by $\delta\mathcal{H} = \sum_i \lambda_i \mathcal{O}_i$. In our case all these operators are marginal, $\Delta_i = 1$. Then the perturbative RG equations are determined by the OPE coefficients [68],

$$d\lambda_i/d\ell = \sum_{jk} c_{ijk} \lambda_j \lambda_k. \quad (\text{C2})$$

We have 15 operators $\mathcal{O}_A = (\psi^\dagger T^A \psi)(f^\dagger T^A f)$ with T_A given in Eq. (14). PH symmetry reduces this to 10 operators. We can gain further insight into the properties of \mathcal{O}_A by analyzing its two factors. In Sec. IID 1 we defined $M^{ab} = f^\dagger T^{ab} f$ and $J^{ab} = \psi^\dagger T^{ab} \psi$, such that $A \in (ab)$ ($a, b = 1, \dots, 5$, $a < b$). The impurity operators M^{ab} satisfy $[M^{ab}, M^{cd}] = -i(\delta_{bc} M^{ad} - \delta_{ac} M^{bd} - \delta_{bd} M^{ac} + \delta_{ad} M^{bc})$. The J^{ab} operators satisfy a similar OPE. This can

be seen if we define a vector of Majorana fields $\vec{\xi}$ via

$$\vec{\xi} = (\chi_{s+}, -\chi_{s-}, \chi_{sf+}, \chi_{f-}, \chi_{f+}, -\chi_{sf-}, \chi_{c+}, \chi_{c-}). \quad (\text{C3})$$

By explicitly using the EK bosonization and refermionization one can show that $J^{ab} = i\xi_a \xi_b$ ($a, b = 1, \dots, 6$). The OPE of the J^{ab} 's then follows from Wick's theorem, and from this one can obtain the OPE satisfied by the \mathcal{O}_A operators, leading to the RG equation [Eq. (18)].

Numerical integration

In Fig. 7 we integrated Eq. (18) starting with anisotropic finite values of the ten PH symmetric couplings. We see a flow to the isotropic SO(5) fixed point.

-
- [1] L. L. Sohn, L. P. Kouwenhoven, and G. Schön, *Mesoscopic Electron Transport* (Springer, Berlin, 2013), Vol. 345.
- [2] R. Wilkins, E. Ben-Jacob, and R. C. Jaklevic, *Phys. Rev. Lett.* **63**, 801 (1989).
- [3] D. Goldhaber-Gordon, H. Shtrikman, D. Mahalu, D. Abusch-Magder, U. Meirav, and M. Kastner, *Nature (London)* **391**, 156 (1998).
- [4] W. Van der Wiel, S. De Franceschi, T. Fujisawa, J. Elzerman, S. Tarucha, and L. Kouwenhoven, *Science* **289**, 2105 (2000).
- [5] S. M. Cronenwett, T. H. Oosterkamp, and L. P. Kouwenhoven, *Science* **281**, 540 (1998).
- [6] S. M. Cronenwett, H. J. Lynch, D. Goldhaber-Gordon, L. P. Kouwenhoven, C. M. Marcus, K. Hirose, N. S. Wingreen, and V. Umansky, *Phys. Rev. Lett.* **88**, 226805 (2002).
- [7] K. A. Matveev, *Phys. Rev. B* **51**, 1743 (1995).
- [8] A. Furusaki and K. A. Matveev, *Phys. Rev. B* **52**, 16676 (1995).
- [9] Y. Oreg and D. Goldhaber-Gordon, *Phys. Rev. Lett.* **90**, 136602 (2003).
- [10] R. Potok, I. Rau, H. Shtrikman, Y. Oreg, and D. Goldhaber-Gordon, *Nature (London)* **446**, 167 (2007).
- [11] A. Keller, L. Peeters, C. Moca, I. Weymann, D. Mahalu, V. Umansky, G. Zaránd, and D. Goldhaber-Gordon, *Nature (London)* **526**, 237 (2015).
- [12] I. Affleck and A. W. W. Ludwig, *Phys. Rev. B* **48**, 7297 (1993).
- [13] M. Pustilnik, L. Borda, L. I. Glazman, and J. von Delft, *Phys. Rev. B* **69**, 115316 (2004).
- [14] M. Vojta, *Philos. Mag.* **86**, 1807 (2006).
- [15] A. I. Tóth, L. Borda, J. von Delft, and G. Zaránd, *Phys. Rev. B* **76**, 155318 (2007).
- [16] A. I. Tóth and G. Zaránd, *Phys. Rev. B* **78**, 165130 (2008).
- [17] E. Sela, A. K. Mitchell, and L. Fritz, *Phys. Rev. Lett.* **106**, 147202 (2011).
- [18] K. Le Hur and P. Simon, *Phys. Rev. B* **67**, 201308(R) (2003).
- [19] K. Le Hur, P. Simon, and L. Borda, *Phys. Rev. B* **69**, 045326 (2004).
- [20] F. B. Anders, E. Lebanon, and A. Schiller, *Phys. B: Cond. Matt.* **359**, 1381 (2005).
- [21] S. Florens and A. Rosch, *Phys. Rev. Lett.* **92**, 216601 (2004).
- [22] P. Simon, J. Salomez, and D. Feinberg, *Phys. Rev. B* **73**, 205325 (2006).
- [23] Y. Liu, X. Yang, X. Fan, and Y. Xia, *J. Phys.: Condens. Matter* **20**, 135226 (2008).
- [24] A. Carmi, Y. Oreg, M. Berkooz, and D. Goldhaber-Gordon, *Phys. Rev. B* **86**, 115129 (2012).
- [25] A. K. Mitchell and E. Sela, *Phys. Rev. B* **85**, 235127 (2012).
- [26] C. J. Bolech and N. Shah, *Phys. Rev. Lett.* **95**, 036801 (2005).
- [27] A. K. Mitchell, D. E. Logan, and H. R. Krishnamurthy, *Phys. Rev. B* **84**, 035119 (2011).
- [28] K. Kikoin and Y. Oreg, *Phys. Rev. B* **76**, 085324 (2007).
- [29] P. L. S. Lopes, I. Affleck, and E. Sela, *Phys. Rev. B* **101**, 085141 (2020).
- [30] Y. Komijani, *Phys. Rev. B* **101**, 235131 (2020).
- [31] Z. Iftikhar, S. Jezouin, A. Anthore, U. Gennser, F. Parmentier, A. Cavanna, and F. Pierre, *Nature (London)* **526**, 233 (2015).
- [32] Z. Iftikhar, A. Anthore, A. Mitchell, F. Parmentier, U. Gennser, A. Ouerghi, A. Cavanna, C. Mora, P. Simon, and F. Pierre, *Science* **360**, 1315 (2018).
- [33] A. Anthore, Z. Iftikhar, E. Boulat, F. D. Parmentier, A. Cavanna, A. Ouerghi, U. Gennser, and F. Pierre, *Phys. Rev. X* **8**, 031075 (2018).
- [34] A. K. Mitchell, L. A. Landau, L. Fritz, and E. Sela, *Phys. Rev. Lett.* **116**, 157202 (2016).
- [35] L. A. Landau, E. Cornfeld, and E. Sela, *Phys. Rev. Lett.* **120**, 186801 (2018).
- [36] G. A. R. van Dalum, A. K. Mitchell, and L. Fritz, *Phys. Rev. B* **102**, 041111(R) (2020).
- [37] T. K. T. Nguyen and M. N. Kiselev, *Phys. Rev. Lett.* **125**, 026801 (2020).
- [38] J.-Y. M. Lee, C. Han, and H.-S. Sim, *Phys. Rev. Lett.* **125**, 196802 (2020).
- [39] L. Borda, G. Zaránd, W. Hofstetter, B. I. Halperin, and J. von Delft, *Phys. Rev. Lett.* **90**, 026602 (2003).
- [40] P. Jarillo-Herrero, J. Kong, H. S. Van Der Zant, C. Dekker, L. P. Kouwenhoven, and S. De Franceschi, *Nature (London)* **434**, 484 (2005).
- [41] A. Makarovski and G. Finkelstein, *Phys. B: Condens. Matter* **403**, 1555 (2008).
- [42] A. Keller, S. Amasha, I. Weymann, C. Moca, I. Rau, J. Katine, H. Shtrikman, G. Zaránd, and D. Goldhaber-Gordon, *Nat. Phys.* **10**, 145 (2014).
- [43] G. Zaránd, A. Brataas, and D. Goldhaber-Gordon, *Solid State Commun.* **126**, 463 (2003).

- [44] T. Sato and M. Eto, *Phys. E* **29**, 652 (2005).
- [45] R. López, D. Sánchez, M. Lee, M.-S. Choi, P. Simon, and K. Le Hur, *Phys. Rev. B* **71**, 115312 (2005).
- [46] E. Lebanon, A. Schiller, and F. B. Anders, *Phys. Rev. B* **68**, 155301 (2003).
- [47] E. Lebanon, A. Schiller, and F. B. Anders, *Phys. Rev. B* **68**, 041311(R) (2003).
- [48] F. B. Anders, E. Lebanon, and A. Schiller, *Phys. Rev. B* **70**, 201306(R) (2004).
- [49] A. K. Mitchell, A. Liberman, E. Sela, and I. Affleck, *Phys. Rev. Lett.* **126**, 147702 (2021).
- [50] J. Ye, *Phys. Rev. B* **56**, R489(R) (1997).
- [51] A. Iucci and C. J. Bolech, *Phys. Rev. B* **77**, 195113 (2008).
- [52] C. J. Bolech and A. Iucci, *Phys. Rev. Lett.* **96**, 056402 (2006).
- [53] A. C. Hewson, *The Kondo Problem to Heavy Fermions*, Cambridge Studies in Magnetism (Cambridge University Press, Cambridge, UK, 1993).
- [54] H. Georgi, *Lie Algebras in Particle Physics: From Isospin to Unified Theories* (CRC Press, Boca Raton, FL, 2018).
- [55] C. Itoi, S. Qin, and I. Affleck, *Phys. Rev. B* **61**, 6747 (2000).
- [56] V. J. Emery and S. Kivelson, *Phys. Rev. B* **46**, 10812 (1992).
- [57] G. Zarand and J. von Delft, *Phys. Rev. B* **61**, 6918 (2000).
- [58] J. von Delft and H. Schoeller, *Ann. Phys.* **7**, 225 (1998).
- [59] J. von Delft, G. Zaránd, and M. Fabrizio, *Phys. Rev. Lett.* **81**, 196 (1998).
- [60] E. Sela and I. Affleck, *Phys. Rev. Lett.* **102**, 047201 (2009).
- [61] I. Affleck, *Nucl. Phys. B* **336**, 517 (1990).
- [62] I. Affleck and A. W. Ludwig, *Nucl. Phys. B* **360**, 641 (1991).
- [63] G. Zaránd, C.-H. Chung, P. Simon, and M. Vojta, *Phys. Rev. Lett.* **97**, 166802 (2006).
- [64] A. K. Mitchell, E. Sela, and D. E. Logan, *Phys. Rev. Lett.* **108**, 086405 (2012).
- [65] N. Hartman, C. Olsen, S. Lüscher, M. Samani, S. Fallahi, G. C. Gardner, M. Manfra, and J. Folk, *Nat. Phys.* **14**, 1083 (2018).
- [66] E. Sela, Y. Oreg, S. Plugge, N. Hartman, S. Lüscher, and J. Folk, *Phys. Rev. Lett.* **123**, 147702 (2019).
- [67] Y. Kleeorin, H. Thierschmann, H. Buhmann, A. Georges, L. W. Molenkamp, and Y. Meir, *Nat. Commun.* **10**, 5801 (2019).
- [68] J. Cardy, *Scaling and Renormalization in Statistical Physics* (Cambridge University Press, Cambridge, U.K., 1996), Vol. 5.